Title

Structure specific amyloid precipitation in biofluids

Author list

M. Rodrigues[1,2], P. Bhattacharjee [3,4], A. Brinkmalm[3,4], D. T. Do[5], C. M. Pearson[5], S. De[1,2,6], A. Ponjavic[1,7,8], J. A. Varela[1,9], K. Kulenkampff[1,2], I. Baudrexel[1], D. Emin[1,2], F. S. Ruggeri[1,10,11], J. E. Lee[1,12], A. R. Carr[1], T. P. J. Knowles[1], H. Zetterberg[3,4,13,14], T. N. Snaddon[5*], S. Gandhi[13,15*], S. F. Lee[1*] and D. Klenerman[1,2*]

Affiliations

[1] *Department of Chemistry, University of Cambridge, Lensfield Road, Cambridge, CB2 1EW, UK*

[2] *UK Dementia Research Institute, University of Cambridge, Cambridge, CB2 0XY, UK.*

[3] *Department of Psychiatry and Neurochemistry, Institute of Neuroscience and Physiology, the Sahlgrenska Academy at the University of Gothenburg, S-431 80 Mölndal, Sweden*

[4] *Clinical Neurochemistry Laboratory, Sahlgrenska University Hospital, Mölndal, Sweden*

[5] *Department of Chemistry, Indiana University, 800 E. Kirkwood Ave. Bloomington, IN 47405, USA.*

[6] *Sheffield Institute for Translational Neuroscience, University of Sheffield, Western Bank, Sheffield, S10 2TN, UK*

[7] *School of Physics and Astronomy, University of Leeds, Woodhouse, Leeds, LS2 9JT, UK*

[8] School of Food Science and Nutrition, University of Leeds, Woodhouse, Leeds, LS2 9JT, UK

[9] *School of Physics and Astronomy, University of St Andrews, North Haugh, St Andrews, KY16 9SS, UK*

[10] *Laboratory of Organic Chemistry, Wageningen University & Research, Stippeneng 4, 6703 WE, The Netherlands*

[11] *Physical Chemistry and Soft Matter, Wageningen University & Research, Stippeneng 4, 6703 WE, The Netherlands*

[12] *School of Chemistry, University of Edinburgh, Joseph Black Building, David Brewster Rd, Edinburgh, EH9 3FJ UK*

[13] *Department of Neurodegenerative Disease, UCL Institute of Neurology, London, WC1N 3BG, UK*

[14] *UK Dementia Research Institute at UCL, Gower Street, London, WC1E 6BT, UK*

[15] *The Francis Crick Institute, 1 Midland Road, King's Cross, London, NW1 1AT, UK*

* Joint corresponding authors

Abstract

The composition of soluble toxic protein aggregates formed in vivo is currently unknown in neurodegenerative diseases, due to their ultra-low concentration in human biofluids and their high degree of heterogeneity. Here we report a method to capture amyloid containing aggregates in human biofluids in an unbiased way, a process we name amyloid precipitation (AP). We use a structure-specific chemical dimer; a Y shaped, bioinspired small molecule with two capture groups for AP to increase affinity. Our capture molecule for amyloid precipitation (CAP-1), consists of a derivative of Pittsburgh compound B (dimer) to target the cross β-sheets of amyloids and a biotin moiety for surface immobilization. By coupling CAP-1 to magnetic beads, we demonstrate that we can target the amyloid structure of all protein aggregates present in human cerebrospinal fluid, isolate them for analysis and then characterise them using single-molecule fluorescence imaging and mass spectrometry. Amyloid precipitation enables unbiased determination of the molecular composition and structural features of the in vivo aggregates, formed in neurodegenerative diseases.

Main Text

Introduction

α-Synuclein, amyloid-β and tau are examples of proteins that self-aggregate in cross β-sheets motifs, and are present in Lewy bodies, amyloid plaques, and tau tangles, respectively[1]. These cross β-sheets (or amyloid structures) are found in the brains of people with neurodegenerative diseases such as Parkinson's and Alzheimer's disease[2–4]. Importantly, brain extracts containing misfolded amyloid-β from patients with Alzheimer's disease (AD) and preformed α-synuclein fibrils induced cerebral β-amyloidosis and α-synuclein propagation, respectively and associated pathologies in mice[5–8]. On the other hand, depletion of aggregates from an AD brain suppressed *in vivo* seeding capability[9] reinforcing the idea that the induction of pathology is likely governed by the structure and concentration of the aggregate seeds[10,6] and highlights the importance of studying the aggregated protein as opposed to its monomeric counterpart.

The exact mechanism by which protein aggregates lead to progressive loss of neuronal cells and result in subsequent pathophysiologic effects like dementia and movement disorders remains poorly understood. It is known that subtle differences in amino acid content result in major structural changes that have an impact in the pathophysiology of these diseases[11–14]. Also, *in vitro* studies have revealed that protein aggregation is a dynamic process where a wide range of aggregates with variable sizes[1] and hydrophilicities[15] are formed, and that the aggregates become more toxic when they acquire cross β-sheets structure[1,16]. We have previously studied the aggregation of α-synuclein in detail using super-resolution imaging and single molecule fluorescence[15–18]. Aggregation proceeds by the formation of small soluble aggregates which undergo slow structural conversions to small oligomeric species with increased β-sheet structure over 24 hours which are cytotoxic to cells[16,17]. Aggregates with β-sheet structure were also shown to be more effective at membrane permeabilisation leading to increased cell death[19]. Other studies showed that thioflavin T (ThT) active aggregates of α-synuclein interact with ATP synthase and increase the probability of the opening of the permeability transition pore of mitochondria ultimately leading to cell death[20]. Thus,

ThT active aggregates of α-synuclein are toxic to cells by a number of mechanisms. ThT active aggregates are formed early in the aggregation reaction (from 1 hour) together with non ThT active species[15]. Both species are spherically-symmetric and smaller than ~50 nm in size, and they are clearly distinct from high aspect ratio and longer fibrils formed at later times (27 hour) which also have a different surface hydrophobicity. The fibrils are also much more highly ordered than the ThT active species that form initially, as measured using fluorescence anisotropy, providing further evidence for a structural conversion[18]. Overall these experiments show that oligomeric non-fibrillar ThT active species form early in the aggregation process with distinct properties from fibrils and are toxic to cells by a variety of mechanisms.

These oligomeric aggregates (< 200 nm) of α-synuclein as well aggregates of amyloid-β (Aβ) and tau are implicated in cellular cytotoxity[20–26] . Moreover, it was recently reported that small soluble amyloid-β aggregates induced extensive membrane permeability while larger β-sheet containing aggregates were most effective at causing an inflammatory response in microglia cells[25]. These findings were replicated in a recent study of the aggregates present in cerebrospinal fluid (CSF) of patients at different stages of AD[27]. The aggregates in the CSF of mild cognitively impaired patients induced more membrane permeabilisation, while larger β-sheet aggregates present in the CSF of AD patients were more effective at inducing inflammation[27]. Together these studies reinforce the idea that aggregates of different size and structure trigger different toxic mechanisms and that the relative proportion of these different aggregates change during the development of the disease.

It is now understood that AD develops before the manifestation of clinical symptoms, so it is important to develop new diagnostic methods in readily available biofluids such as blood, urine and CSF. In particular, CSF is one of the major clearance systems and provides an accessible biofluid that can be used to assess extracellular protein aggregates. However, the protein aggregates present in CSF are at very low (sub-picomolar) concentrations and they are very heterogeneous in size[28,29].

These two factors have significantly hindered the development of suitable tools to isolate and study protein aggregates from human biofluids. New methods are needed to isolate and characterise the low levels of aggregates present in human biofluids in order to better understand how compositional and structural differences in these aggregates impact cellular toxicity and contribute to disease pathogenesis. This is a fundamental step toward the development of effective therapeutic strategies and for early diagnosis of disease.

Until recently, proteins aggregates implicated in neurodegeneration have largely been characterised using capture techniques based on antibodies or aptamers [30–33]. However, both antibody and aptamer capture strategies have a fundamental limitation that they only target aggregates of a selected protein as well as having other problems such as epitope accessibility on misfolded proteins, inefficient targeting if the aggregated proteins contains post-translational modifications, and difficulties to recognise aggregates composed by oligomers formed by more than one type of protein[34,35]. To address these issues we have developed a structure specific chemical dimer designed to selectively bind cross β-sheet motifs instead of a specific protein epitope, allowing detection of the range of protein aggregates associated with neurodegenerative diseases[29,36] in an unbiased fashion. We have named this new molecule capture molecule for amyloid precipitation (CAP-1). Protein aggregates can be precipitated from solution by attaching CAP-1 to magnetic beads, which we refer to as amyloid precipitation (AP). This AP approach enables an array of molecular and cellular techniques, ranging from single-molecule imaging to cytotoxicity studies, to be performed to characterise the structural and functional properties of protein aggregates.

Results

Rational design and characterization of a bio-inspired amyloid-specific probe

The design of CAP-1 was inspired by the structure of antibodies due to their natural high affinity to target specific molecules, based on their Y-shaped structure with two binding sites. This chemical molecule is designed to recognise β-sheet structures with high affinity and is based on a dimer of benzothiazole derivatives. This derivative contains structural elements of thioflavin T (ThT) for its photophysical and optical properties[36,37], for detection of aggregate binding. It also contains structural elements of Pittsburgh compound B (PiB) for its increased affinity to β-sheet structures compared with ThT, namely the lack of two methyl groups and charge in the benzothiazole group of PiB[38,39], for efficient capture of β-sheet containing aggregates. A recent study has used a similar approach to develop a multivalent PET ligand to image Aβ aggregates in the brain[40].

The synthesis of CAP-1 was achieved using established methods; see Fig. 1a for structure and SI.1-9 for synthesis details. The trimeric species has two β-sheet binding sites for increased avidity (as previously described for a dimeric version of ThT[41]) and has a third site for immobilisation, in this specific implementation *via* biotin – streptavidin binding.

After initial spectral characterisation of CAP-1, $\lambda_{ex\text{-}em}$ 355-440 nm (SI.10) and solubility measurements (SI.11) we evaluated the binding of CAP-1 to α-synuclein monomers, oligomers and fibrils (Fig. 1b-d). CAP-1 binds to oligomers as well as fibrils but not monomers, see Fig.1b-d and SI.12. CAP-1, like ThT[42], is suitable for total internal reflection fluorescence microscopy (TIRFM), and can be used to monitor the aggregation reaction, from small early stage aggregates ($t > 4h$) to long mature fibrils ($t > 24h$), Fig.1c-d. Kinetic studies of the α-synuclein aggregation in the presence of CAP-1 or ThT showed similar changes in fluorescence, as expected (SI.13).

α-synuclein was selected as the model amyloid protein throughout this work but we also achieved similar results using other amyloid proteins such as $A\beta_{42}$ and tau aggregates (SI.14), with comparable ratios of signal to background. The binding of CAP-1 to these protein aggregates further supports the specificity towards cross β-sheet regardless of protein sequence, highlighting the value of using CAP-1 to target a 'structural epitope'. Such a non-biased approach is key since the composition of *in vivo* aggregates remains elusive.

Finally, we determined the binding affinity of CAP-1 to α-synuclein and compared this affinity with that of ThT (Fig. 1e) using bulk fluorescence and sonicated fibrils (average length 200 nm), to avoid heterogeneity in the structure and size of the aggregates (see SI.15). Using an initial concentration of 100 nM α-synuclein (monomer equivalent) we obtained a K_d (CAP-1) = 14 ± 5 nM and K_d (ThT) = 1400 ± 140 nM (SI.16), representing a 280-fold increase in affinity of CAP-1 compared to ThT. Dissociation constants often depend on the approach used and previous studies reported K_d of ThT for α-synuclein fibrils from 588 nM to 100 μM[43,44]. The significant increase in CAP-1 affinity towards amyloids compared to ThT can be explained by the combination of two key factors: CAP-1 being a dimer, as previously described avidity increases affinity[41] and the absence of the *N*-methylated benzothiazole moiety (SI.1) as seen for PiB[38,39]. The K_d for a monovalent version of CAP-1 was 35 ± 12 nM confirming that dimerisation increased the binding affinity (SI.16) The K_d for CAP-1 for $A\beta_{40}$ was 17 ± 8 nM, supporting the specificity of CAP-1 binding to cross β-sheet aggregates (SI.16). The K_d of ThT for $A\beta_{40}$ was reported to be 2.3 μM[41], again demonstrating the increase of binding affinity of CAP-1 over ThT.

Capture of protein aggregates using CAP-1 – Method of amyloid-precipitation

Following the characterization of CAP-1 binding to α-synuclein, we designed a protocol for isolation of protein aggregates from solution, which we have named amyloid precipitation (AP). The schematic of AP is outlined in Fig. 2a-b. After the conjugation of CAP-1 with magnetic streptavidin-coated beads (Fig. 2a), the beads are added to a solution containing protein aggregates such as recombinant α-synuclein solution or a biofluid. After 2h at 4°C with gentle mixing, the beads are separated using a magnet and both fractions ('beads' and 'depleted') are analysed by TIRFM (Fig. 2c) and bulk fluorescence (Fig. 2d). We found that there was some clumping of the beads in the absence of protein, but the presence of proteins prevented clumping allowing us to perform AP.

Fig. 2c shows conjugated beads with CAP-1 after AP using α-synuclein fibrils (right) or PBS (left). The presence of fibrils (right panel) attached to the beads is visible by the 'hairy' appearance of the beads and highlighted in the magnified bead, and contrasts with the plain look of beads without protein (left panel). Despite the heterogeneous bead-to-fibril attachment, some beads contain many small fibrils and other fewer but longer fibrils, there is a significant difference in the diameter (measured as fluorescence intensity profile) between beads in the presence or absence of α-synuclein fibrils, 105 nm (p = 0.0002) confirming the successful binding of fibrils to beads (see SI.17).

In Fig. 2d we tested the efficacy of AP towards α-synuclein fibrils (purple) *versus* α-synuclein monomers (orange) (see SI.18 for representative fluorescent spectra of both fractions). The difference between beads incubated with α-synuclein fibrils (100%, purple) and beads with α-synuclein monomers (33%, orange) highlights the absence of cross β-sheet in the monomeric solution and corresponds to the fluorescence of CAP-1 alone. The fluorescence intensity for the samples, beads+CAP-1+monomers (orange) and beads+CAP-1+PBS (grey), is the same for both beads and supernatant, confirming that CAP-1 does not bind to monomers. The low fluorescence

intensity detected for the supernatant of both samples, 11% for fibrils and 3% for monomers, respectively, reflects the presence of residual CAP-1 molecules released from the beads during the incubation and as expected is higher for the sample containing fibrils. Overall, the fluorescence increase between the supernatant (11%) and beads (100%) for the α-synuclein fibrils sample demonstrates the successful pulldown (and concentration) of aggregates by the beads.

In both TIRFM (Fig. 2c) and bulk (Fig. 2c) measurements, detection of protein aggregates is based on CAP-1 intrinsic fluorescence, highlighting its ability to strongly bind (capture) aggregates and work as optical readout for the presence of β-sheets. We also used atomic force microscopy (AFM), an orthogonal non-optical technique, to confirm the successful binding of α-synuclein fibrils to CAP-1-beads (SI.19). As shown in the 3D (height) image fibrils localize preferentially close to the beads (SI.19a), once more demonstrating the preference of protein aggregates to CAP-1 coated beads.

Until now, we have used mature α-synuclein fibrils (sonicated 200 nm, non-sonicated >1 μm) as a model of protein aggregation to test AP. However, in biological fluids such as cerebrospinal fluid (CSF) the aggregates present are smaller. These 'early stage' soluble aggregates, or oligomers, have been shown to be much smaller that the optical diffraction limit (~250 nm)[42] and differ in size, shape and structure from fibrils using higher resolution methods such as AD-PAINT[15] and AFM[45]. For this reason we used α-synuclein aggregates collected at the 8 hour time point to maximize the number of these oligomers[15,16] and to validate the AP method for use in a biological context. We used EM to characterize aggregates present at 8h (SI.22) and confirmed their sub-diffraction limit size (~30 nm). The results in Fig. 2e show the number of fluorescent puncta before and after amyloid precipitation, $6.0 \times 10^{-2}/\mu m^2$ and $3.6 \times 10^{-4}/\mu m^2$, respectively (see SI.21 TIRFM images). In the presence of CAP-1 the number of protein aggregates in solution after pulldown is reduced to background levels (Fig. 2e, grey column - $4.2 \times 10^{-4} \pm 2.3 \times 10^{-4} /\mu m^2$). In the absence of CAP-1

there was partial removal of aggregates (see SI.21) suggesting unspecific binding to the beads but negligible compared to the virtually complete depletion, 99.4%, in the presence of CAP-1. Overall, these experiments demonstrate that AP can be used to capture α-synuclein oligomers.

Next, we investigated the use of mass spectrometry (MS) to quantify the amount of α-synuclein enriched on the beads after pulldown as MS will allow identification of molecular composition of the amyloids captured using AP. For this, we used high-resolution parallel reaction monitoring (PRM) mass spectrometry (MS). After AP, α-synuclein was eluted from the beads and digested using trypsin, converting full length α-synuclein into small peptides, namely α-syn$_{13-21}$, α-syn$_{35-43}$, α-syn$_{46-58}$, α-syn$_{61-80}$, and α-syn$_{81-96}$. In order to confirm the specificity of CAP-1, we compared the presence and absence of CAP-1 during the AP. In the presence of CAP-1 the amount of individual tryptic α-synuclein peptides recovered was 5 to 13 times higher, depending on the peptide, than without CAP-1 (SI.23). This is in agreement with TIRFM results (Fig. 2e). The PRM-MS spectrum in Fig. 2f shows the relative abundance of α-synuclein$_{13-21}$ peptide fragment ion (y_n) fragment ions spectrum in the presence (right) and absence (left) of CAP-1.

Amyloid-precipitation followed by PRM mass spectrometry of α-synuclein spiked in human CSF

AP is an unbiased method to capture amyloid protein from solution, allowing subsequent mass spectrometry identification of proteins present in such aggregates[46,47]. As CSF is a complex biofluid made of more than two thousand different proteins[48], we firstly determined the sensitivity of CAP-1-beads to capture known amounts of α-synuclein spiked in CSF.

Increasing amounts of either purified α-synuclein monomers (t = 0 hours) or α-synuclein mixture of monomers (>95%) and oligomers (<5%)[16] (t = 8 hours), were spiked in control CSF, see Fig. 3a for the outline of the experiment and SI.25 for TIRFM representative images. After AP, the beads were trypsin-digested and analysed by PRM-MS. In Fig. 3b the amount of α-synuclein$_{13\text{-}21}$ peptide recovered as a function of the initial α-synuclein concentration spiked is shown. Naturally occurring α-synuclein oligomers present in CSF were undetectable (see Table 3-8 for list of proteins pulled down). For concentrations equal to and below 1 nM, monomers were not detected, while in 1 nM of mixed species 28 femtomoles (28 pM) of α-syn$_{13\text{-}21}$ captured were detected (SI.24 for other peptides). For α-synuclein concentrations higher than 1 nM, the increase in α-syn$_{13\text{-}21}$ detected is linear and about three times higher for the mixed species sample than for the monomers (Fig. 3b). CAP-1-beads captured 0.6% of total α-synuclein monomers (orange) spiked in CSF and 2.3% of total α-synuclein mixture (monomers >95% and oligomers <5%, purple). This means that almost no monomers in solution are captured while approximately 50% (2.3% out of <5%) of the oligomers added to CSF are captured. For this reason, the 3-fold change in the total amount of α-syn$_{13\text{-}21}$ recovered (Fig. 3b) represents a large difference in capture affinity between the monomer which is present at high concentration and low concentration of aggregated α-synuclein. This result confirms the specificity of AP in capturing protein aggregates compared to the monomers in complex biofluids such as CSF.

The proteins captured using CAP-1 beads should be enriched in amyloid prone proteins or contain proteins in the CSF that bind amyloid proteins[35]. Using PASTA 2.0[49] and RFAmyloid[50], two highly cited web servers for the prediction of protein aggregation from sequence we observed an increase in the total number of amyloid-prone proteins when using CAP-1 compared to unmodified beads (see SI Table 9). As expected, in the presence of CAP-1 there is an increase in the total β-strand content of captured proteins (25-26%) compared to not using the capture molecule (19%), providing further computational evidence of the ability of CAP-1 to select β-sheet containing proteins (see Table 1 and 2).

To evaluate the efficiency of AP in removing toxic amyloid species from CSF we used a sensitive membrane permeability assay previously developed[22] (see Fig. 3c for outline of the experiment). CSF is diluted in a solution containing Ca^{2+} ions and then added to liposomes containing a Ca^{2+}-dependent dye. If CSF contains amyloids/oligomers that cause membrane permeability, Ca^{2+} ions enters the liposome resulting in increased fluorescence. The increase in signal when the concentration of Ca^{2+} ions equals the bath concentration is determined at the end of the experiment by adding ionomycin. This corresponds to 100 % Ca^{2+} ion entry and means that the measurement is quantitative with a scale from 0-100 %. In Fig. 3d, the average Ca^{2+} influxes for CSF before AP (purple), CSF after AP ('depleted' fraction) (white) and CSF after AP without CAP-1 (white with purple dots) using the same CSF as in Fig. 3b it is plotted. AP removed most of the CSF proteins responsible for Ca^{2+} influx, reducing membrane permeability from 27% to 6%. There is some depletion in the absence of CAP-1 due to non-specific binding to the beads[51–53]. Having established that AP is able to remove amyloid proteins from control CSF (Fig. 3b-d), we then decided to use CSF from Parkinson's disease (PD) patients in a separate set of experiments (Fig. 3e-f). TIRFM images showed a significant decrease in the number of ThT active species after AP Fig. 3g (left panels) and we found that there was a reduction of ~50% in Ca^{2+} influx. This demonstrates that AP can capture amyloid aggregates from PD CSF. It is worth noting that there is non-specific binding

to the beads without CAP-1 that leads to some aggregate capture and a small reduction in membrane permeability (Fig. 3d-e middle column).

Conclusions

Protein aggregates have been known to be implicated in neurodegenerative diseases for more than three decades[54]. Yet, despite much progress there are still significant technological limitations in isolating and characterising the intermediate small species that are formed during the development of disease, this is due to the low abundance, small size and, heterogeneity in conformation and composition of the aggregates[55–58]. Traditional immunocapture/immune recognition approaches have improved in being able to target misfolded/aggregated proteins but are not capable of distinguishing between aggregates of different structures that may have very different properties and toxicities[59]. The goal of this work is to design an unbiased method to capture and characterise all the aggregates with a cross β-sheet structure that are present in human biofluids to determine their composition.

In this study, we presented the synthesis and characterisation of a structure specific chemical dimer designed to capture the protein aggregates associated with neurodegeneration from solution. This molecule has been specifically developed to bind and isolate a target molecule based on secondary structure, the presence of β-sheets, using chemical head groups that form the basis of PET ligands[60,61]. Previous studies have made use of dimerised ligands (protein/peptide[62,63] or ThT[41]) as a way to improve binding affinity to a particular target molecule. To the best of our knowledge, this is the first study to exploit the increased affinity of dimerised ligands in order to enable isolation/precipitation of the target species based on its structure rather than its protein composition. The CAP-1 structure was successfully designed and then demonstrated to bind and isolate aggregates with amyloid structure (fibrils of $A\beta_{42}$, tau and α-synuclein), but crucially not monomers, using synthetic aggregates. Furthermore, the K_d for CAP-1 binding $A\beta_{40}$ and α-synuclein fibrils were comparable which suggests that there will be no selective bias in capturing aggregates of different proteins. Importantly we have also demonstrated amyloid precipitation of early aggregates of α-synuclein formed after 8 hours of aggregation, which are predominantly oligomers (SI.21).

Our data (SI.20) shows that most of the oligomers are selectively removed by CAP-1 but not by the beads alone. This is strong evidence that CAP-1 captures oligomers of α-synuclein as well as fibrils.

However, it is also critical to demonstrate translational relevance. *In vivo*, the complexity of the biofluids that surround the CNS (CSF) and the brain tissue itself makes the detection of small amyloids a major challenge[64]. We demonstrated the sensitive detection of amyloid containing aggregates can be performed in CSF by amyloid pulldown using CAP-1, followed by bead digestion and detection by mass spectrometry. We observed an increased number of amyloid-prone proteins when using CAP-1 compared to plain beads and an increase in the total content of β-strand highlighting the strength of our method AP in enriching β-sheet containing proteins (see Table 1 and 2).

An important question to consider is whether CAP-1 will capture toxic aggregates. Our previous work showed that the oligomers formed after a structural conversion to a more proteinase K resistant structure are cytotoxic to neurons[16], and the formation of β-sheet active species has been shown to lead to increased membrane permeabilization[65]. These species were also shown to be ThT active[15] and hence should be captured by CAP-1. We also previously showed that monomers of Aβ or α-synuclein cannot cause membrane permeabilisation but aggregates can[22] and hence it is likely that only protein aggregates (and not monomers) present in CSF cause membrane permeabilisation. Since our experiments using CSF showed that CAP-1 captures the species responsible for membrane permeabilisation and calcium ion entry, then included in the species captured by CAP-1 should be the toxic aggregates present in CSF responsible for disrupting calcium ion homeostasis *in vivo*. This data therefore shows that CAP-1 captures toxic aggregates from CSF. However, we cannot rule out that there will be non-Th T active species that are also toxic and will not be captured by CAP-1 but these species appear not to be the dominant toxic species present in CSF as measured by the membrane permeabilisation assay.

This new capability for unbiased detection and capture of amyloids, coupled with a mass spectrometry approach to provide the molecular composition is a powerful combination because it has the potential to define the amyloids present in the brain, CSF and other biofluids. The ability of disease causing aggregates (containing β-sheets) to cause membrane permeabilization as been previously correlated with their cytotoxic potential[22,25]. Importantly, in AP the beads contain negligible monomers and, since it is possible to remove the captured aggregates from the beads, this approach allows further characterization of the human derived aggregates and cytotoxicity experiments to be performed. Further improvements to the design of the capture molecule are possible by optimising the linker length, head groups and synthesising multimeric molecules to further improve the sensitivity and selectivity of amyloid precipitation[66,67]. This may further increase the affinity of the dimer of CAP-1 over the monomeric version. There may also be significant advantages in this approach in terms of stability and resistance to degradation compared to conventional antibodies[68–70].

One particular advantage of this approach in **the unbiased selection of amyloid conformations** of proteins, regardless of their molecular identity. The appearance of misfolded and aggregated proteins is likely to important in early stage disease, and developing complementary methods that do not require protein specific approaches but structural ones may identify the important biomarker in any disease. This is particularly true as it is the structural conformation that is the biggest determinant of toxicity in disease, and therefore this approach may select for the pathogenic biomarker of disease.

This approach may ultimately lead to early diagnostic tools. The capability to detect β-sheet aggregates present in an unbiased way will allow us to determine which protein aggregates change during the development of AD or PD and hence develop new diagnostic methods for early disease detection. Several studies show that aggregates of Aβ, α-synuclein and tau are present in the human biological fluids such as CSF and serum of patient affected with Alzheimer's (Aβ and Tau) and Parkinson (α-synuclein)[71–74]. Since the aggregation and deposition of these proteins to cross β-sheet

rich aggregates start in the CNS almost 5-15 years before clinical manifestations of disease, detection of these β-sheet rich aggregates hold the promise of developing a long-awaited diagnosis of AD and PD at the clinically asymptomatic stage as well as predict disease progression, and monitor effects of potential drugs.

This approach will also yield insights into disease mechanisms: it provides fundamental information about the role of protein aggregation in human disease allowing one to study how protein homeostasis is disrupted in humans and whether this is due to aggregation of a specific protein such as α-synuclein in PD or more general aggregation of several aggregation prone proteins such as Aβ, tau and α-synuclein and TDP43. It is also not known how the relative amounts of these different aggregates will change during the development of different neurodegenerative diseases. In the latter case differences in the relative amounts of these different proteins in biofluids would define the different diseases. It also may reveal if protein aggregates play a fundamental role in human physiology, since they are present from a young age, or only form as a result of ageing. Addressing all these questions is only possible using an unbiased method that detects all β-sheet aggregates.

In conclusion, we have successfully developed a new molecule inspired by the trimeric shape of an antibody to target all aggregates containing cross β-sheet motifs present in complex biofluids. CAP-1 has two binding sites to improve avidity and a third moiety to enable surface immobilisation and therefore capture of aggregates based on their structure, but not their protein composition. This simple and versatile method allows the identification of molecular components of aggregates, using mass spectrometry. Overall, this structure-based approach will pave the way to understanding the exact molecular species responsible for neurodegeneration in humans and consequently hasten development of simple and robust early diagnosis methods.

Acknowledgements

HZ is a Wallenberg Scholar supported by grants from the Swedish Research Council (#2018-02532), the European Research Council (#681712), Swedish State Support for Clinical Research (#ALFGBG-720931) and the UK Dementia Research Institute at UCL. DK is supported by grants from the European Research Council (#669237), the Royal Society and UK Dementia Research Institute at Cambridge. We thank the Royal Society for the University Research Fellowship to SFL (UF120277), TNS: National Institutes of Health (R01GM121573). Also, Michael J. Fox Grant to SFL and TNS (grant ID: 10200). JAV is supported by the European Research Council with an ERC Starting Grant (804581).

Author Contributions

SFL and TNS designed CAP-1 and DTF and CMP synthesised CAP-1. MR performed all the experiments with CAP-1 alongside with JAV for imaging experiments and analysis, IB for pulldown essay, DE for binding affinity experiments and JEL for beads imaging. AP and ARC helped with imaging analysis and KK prepared aβ_{42} and tau aggregates. SD performed the liposome assays and FSR the AFM measurements. HZ directed the mass spectrometry studies and MR, PB and AB designed and performed the experiments and data analysis. SFL, SG and DK directed the research. MR wrote the first draft of the paper and all authors contributed to discussion and final draft.

Competing Interests

HZ has served at scientific advisory boards for Roche Diagnostics, Wave, Samumed and CogRx, has given lectures in symposia sponsored by Alzecure and Biogen, and is a co-founder of Brain Biomarker Solutions in Gothenburg AB, a GU Ventures-based platform company at the University of Gothenburg (outside submitted work). The remaining authors declare no competing interests.

Figure legends/captions

Figure 1 – Design and characterization of a bio-inspired structure-specific chemical dimer. (**a)** CAP-1 chemical structure. In purple the amyloid binding regions and in blue, biotin used for surface attachment *via* streptavidin binding. (**b**) Illustrative diagram highlighting the selective affinity of CAP-1 to cross β-sheets present in early stage aggregates and fibrils but not in monomers. (**c**) TIRFM images of α-synuclein aggregation at 0h, 8h (red circles highlighting oligomers) and 24h using 5 μM CAP-1 and 2.8 μM α-synuclein, λ_{ex}405 nm. Scale bar = 5 μm, inset scale bar = 2 μm. (**d**) Maximum fluorescence intensity increase of CAP-1 (20 μM) upon binding to 10 μM α-synuclein at different time points of the aggregation reaction using λ_{ex}355 nm. Data are presented as the mean ± s.d. of $n = 2$ independent experiments. One-way ANOVA (p=0.0006) and Tukey's post hoc comparisons (**p<0.0017, ***p=0.0007 and n.s. p>0.05). (**e**) Binding affinity of CAP-1 and ThT to α-synuclein. Increasing amounts of CAP-1 or ThT were added to 100 nM total monomer concentration of sonicated α-synuclein fibrils. Data are presented as the mean ± s.d. of $n = 3$ or $n = 2$ independent experiments for CAP-1 or ThT, respectively. The K_d for ThT was obtained by fitting the experimental points to a hyperbolic curve (specific binding) K_d (ThT) = 1400 ± 132 nM and for CAP-1 a model for binding fluorescent ligands that takes account of the change in fluorescence between bound and unbound molecule was used, K_d (CAP-1) = 14 ± 5 nM. For more details see Supplementary Information Methods.

Figure 2 – Amyloid-precipitation using CAP-1. (**a**) Magnetic Dynabeads coated with streptavidin conjugated with CAP-1 via biotin moiety. (**b**) Outline of the amyloid-precipitation (AP) method. Functionalised beads with CAP-1 are incubated with an amyloid containing solution. After incubation beads bound to proteins aggregates are isolated using a magnet. Both fractions, depleted (supernatant - SN) and enriched fraction (beads) can be analysed by bulk fluorescence and TIRFM. (**c)** TIRFM of Dynabeads Streptavidin C1 coated with CAP-1 and in the presence (right panel) or absence (left panel) of 10 μM α-synuclein fibrils (right panel) using λ_{ex} 405 nm. α-synuclein fibrils can be seen attached to the beads creating a 'hairy' bead look (right panel detail) or in other cases as a single long and thick spike. In the absence of protein aggregates (left panel) beads have a plain look. Scale bar = 3 μm. (**d**) Bulk fluorescence intensity (normalised) of beads (B) and supernatant (SN) after AP using 10 μM α-synuclein, (■) sonicated fibrils (5 days incubation), (■) monomers and (■) PBS only, λ_{ex} 355 nm and λ_{em_max}. SN represents the supernatant or 'depleted' fraction and B the 'beads' fraction. The horizontal green area highlights that the fluorescence of beads+CAP-1+monomers is the same as beads+CAP-1 without protein supporting the idea that CAP-1 does not bind to monomers *i.e*. the fluorescence measured is due to CAP-1 alone. Data are presented as the mean ± s.d. of $n = 2$ independent experiments (each value corresponds to mean of $n = 3$ replicates) and differences between groups were analysed using unpaired two-tailed Student's t test, *p=0.0345, **p=0.0062 and ***p=0.0004. (**e**) Depletion of α-synuclein oligomers (time point 8h of α-synuclein aggregation reaction) by AP and quantification of aggregates left in the supernatant (depleted fraction). Plotted is the fluorescent puncta counts $x10^2/\mu m^2$ for the sample before and after AP using TIRFM. AP captures approximately ~100% of oligomers in solution. Data are presented as the mean ± s.d. of $n = 27$ fields of view per sample for one representative experiment (see SI.21 for TIRFM images) (**f**) Outline of AP followed by on bead digestion. α-synuclein$_{13-21}$ peptide fragment ion (y_2 to y_8) PRM spectrum in the presence (right) and absence (left) of CAP-1, recovered after AP from a solution containing 1 nM total α-synuclein (<50 pM oligomers).

Figure 3 – Amyloid-precipitation of CSF spiked with recombinant α-synuclein oligomers. (**a**) Outline of the experiment. Known amounts of recombinant α-synuclein monomers or mixture of oligomers + monomers (<95%) are spiked into control CSF. (**b**) Quantification of α-synuclein$_{13-21}$ peptide recovered from on-bead digestion after AP using PRM-MS. Results were plotted as amount of α-synuclein$_{13-21}$ peptide recovered in fmol as a function of the initial α-synuclein concentration used for AP in pM from α-synuclein monomers (-●-) and from α-synuclein mixture (oligomers+monomers) (-●-). Data are presented as the mean ± s.d. of $n = 3$ independent experiments. (**c**) Outline of the membrane permeabilization essay. (**d**) Average Ca^{2+} influx in control CSF (CSF used in **b**) before and after AP, and after AP in the absence of CAP-1. Data are presented as the mean ± s.d. of $n > 10$ fields of view per sample for one representative experiment. **e**) Average Ca^{2+} influx of PD CSF sample before and after AP in the presence of CAP-1 and, after AP in the absence of CAP-1. Data are presented as the mean ± s.d. of $n = 5$ (CSF from 5 different patients) and each point corresponds to the mean of $n > 10$ fields of view per sample for one representative experiment. One-way ANOVA ($p<0.0001$) and Tukey's post hoc comparison (****$p<0.0001$, ***$p=0.0002$ and ns>0.05). (**f**) Example of TIRFM image of PD CSF sample before (left) and after (right) AP, λ_{ex}405 nm and 5 μM ThT, scale bar 10 μm.

Figures

Figure 1

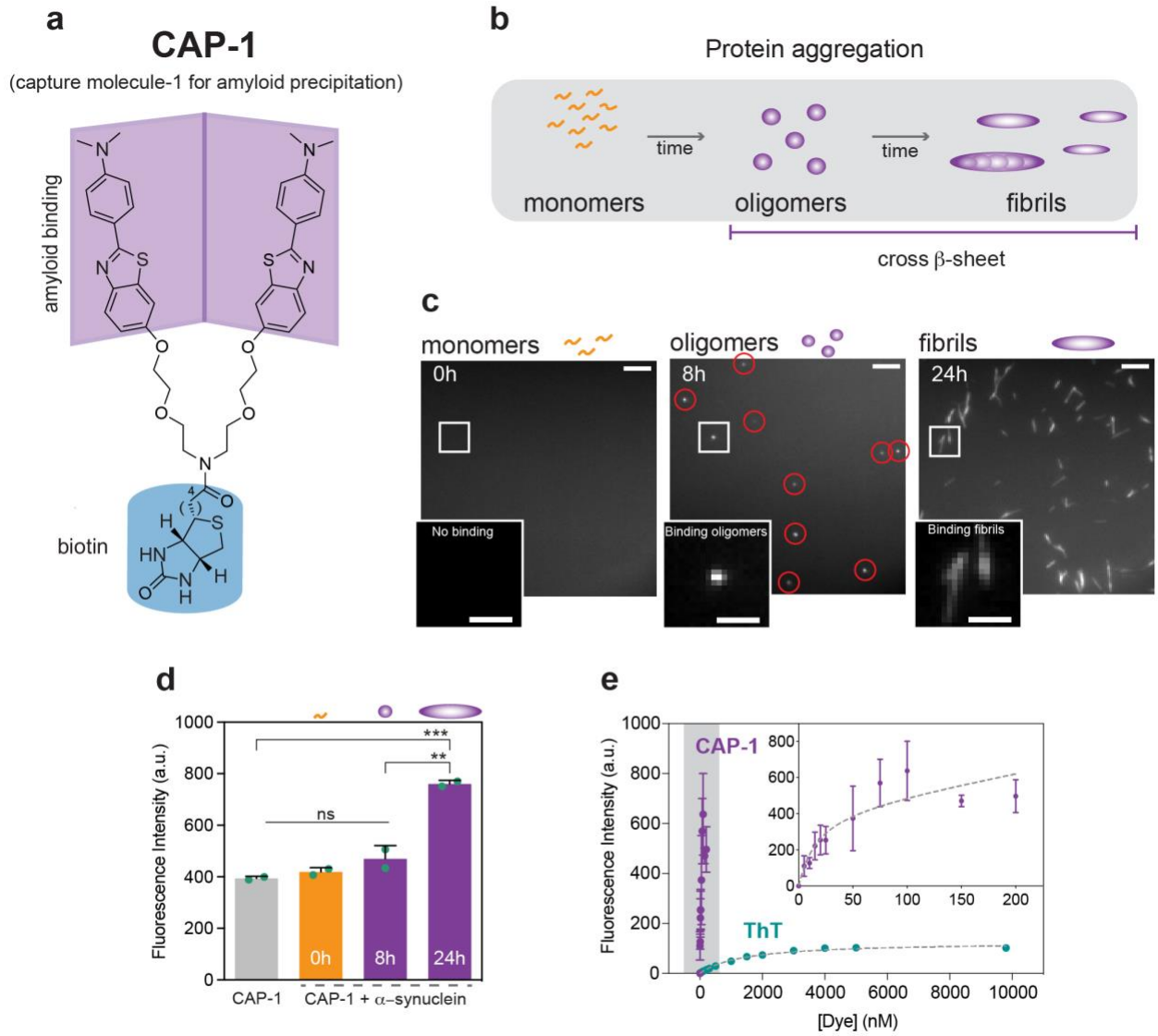

Figure 2

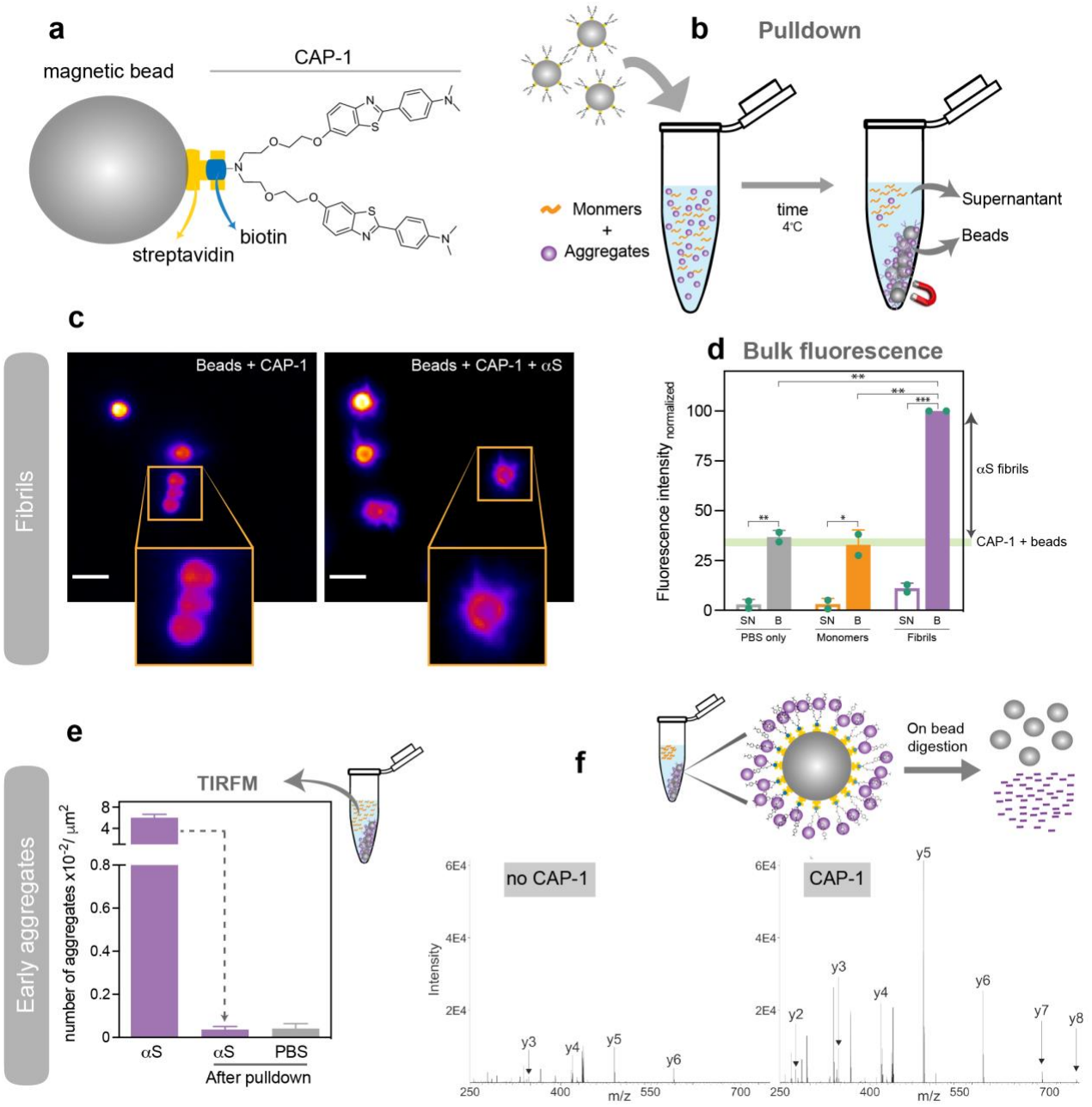
a
magnetic bead
CAP-1
streptavidin
biotin
b
Pulldown
Monmers
+
Aggregates
time
4°C
Supernantant
Beads
c
Fibrils
Beads + CAP-1
Beads + CAP-1 + αS
d
Bulk fluorescence
Fluorescence intensity normalized
αS fibrils
CAP-1 + beads
SN B
PBS only
Monomers
Fibrils
e
Early aggregates
TIRFM
number of aggregates x10-2/ μm2
αS
αS
PBS
After pulldown
f
On bead
digestion
no CAP-1
CAP-1
Intensity
m/z

Figure 3

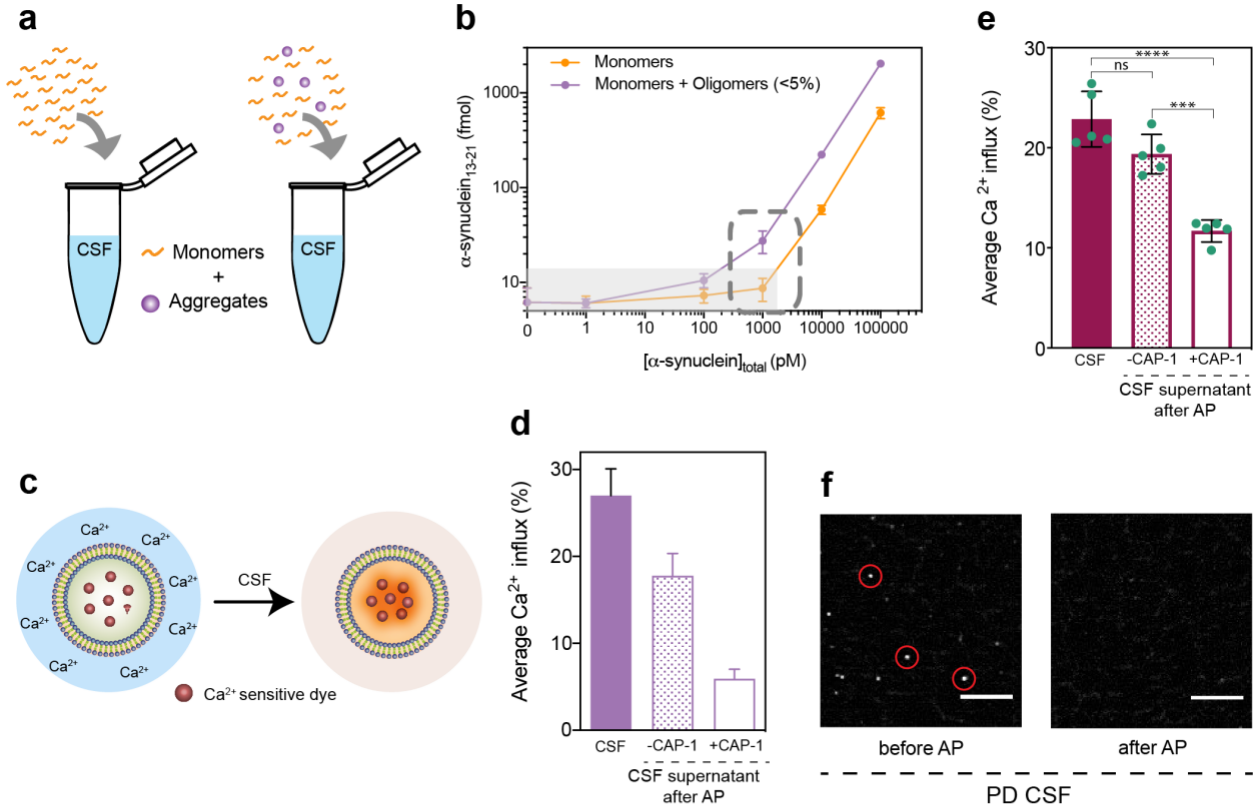
a
CSF
Monomers
+
Aggregates
CSF
b
Monomers
Monomers + Oligomers (<5%)
α-synuclein13-21 (fmol)
[α-synuclein]total (pM)
e
Average Ca 2+ influx (%)
ns
****
***
CSF
-CAP-1
+CAP-1
CSF supernatant
after AP
c
Ca2+
CSF
Ca2+ sensitive dye
d
Average Ca2+ influx (%)
CSF
-CAP-1
+CAP-1
CSF supernatant
after AP
f
before AP
after AP
PD CSF

References

1. Knowles, T. P. J., Vendruscolo, M. & Dobson, C. M. The amyloid state and its association with protein misfolding diseases. *Nature Reviews Molecular Cell Biology* vol. 15 384–396 (2014).
2. Braak, H. *et al.* Pattern of brain destruction in Parkinson's and Alzheimer's diseases. *J. Neural Transm.* **103**, 455–490 (1996).
3. Goedert, M. Alzheimer's and Parkinson's diseases: The prion concept in relation to assembled Aβ, tau, and α-synuclein. *Science.* **349**, 61–69 (2015).
4. Scheltens, P. *et al.* Alzheimer's disease. *Lancet* **388**, 505–517 (2016).
5. Eisele, Y. S. *et al.* Peripherally Applied Aβ-Containing Inoculates Induce Cerebral β-Amyloidosis. *Science.* **330**, 980–982 (2010).
6. Meyer-Luehmann, M. *et al.* Exogenous induction of cerebral β-amyloidogenesis is governed bf agent and host. *Science.* **313**, 1781–1784 (2006).
7. Luk, K. C. *et al.* Intracerebral inoculation of pathological α-synuclein initiates a rapidly progressive neurodegenerative α-synucleinopathy in mice. *J. Exp. Med.* **209**, 975–988 (2012).
8. Karampetsou, M. *et al.* Phosphorylated exogenous alpha-synuclein fibrils exacerbate pathology and induce neuronal dysfunction in mice. *Sci. Rep.* **7**, 1–18 (2017).
9. Duran-Aniotz, C. *et al.* Aggregate-depleted brain fails to induce Aβ deposition in a mouse model of Alzheimer's disease. *PLoS One* **9**, (2014).
10. Morales, R., Bravo-Alegria, J., Duran-Aniotz, C. & Soto, C. Titration of biologically active amyloid-β seeds in a transgenic mouse model of Alzheimer's disease. *Sci. Rep.* **5**, 1–8 (2015).
11. Condello, C. *et al.* Structural heterogeneity and intersubject variability of Aβ in familial and sporadic Alzheimer's disease. *Proc. Natl. Acad. Sci. U. S. A.* **115**, E782–E791 (2018).
12. Lázaro, D. F. *et al.* Systematic Comparison of the Effects of Alpha-synuclein Mutations on Its Oligomerization and Aggregation. *PLoS Genet.* **10**, (2014).
13. Tosatto, L. *et al.* Single-molecule FRET studies on alpha-synuclein oligomerization of Parkinson's disease genetically related mutants. *Sci. Rep.* **5**, 1–12 (2015).
14. Boyer, D. R. *et al.* The α-synuclein hereditary mutation E46K unlocks a more stable, pathogenic fibril structure. *Proc. Natl. Acad. Sci. U. S. A.* **117**, 3592–3602 (2020).
15. Lee, J. E. *et al.* Mapping Surface Hydrophobicity of α-Synuclein Oligomers at the Nanoscale. *Nano Lett.* **18**, 7494–7501 (2018).
16. Cremades, N. *et al.* Direct observation of the interconversion of normal and toxic forms of α-synuclein. *Cell* **149**, 1048–1059 (2012).
17. Iljina, M. *et al.* Kinetic model of the aggregation of alpha-synuclein provides insights into

prion-like spreading. *Proc. Natl. Acad. Sci. U. S. A.* **113**, E1206–E1215 (2016).

18. Varela, J. A. *et al.* Optical Structural Analysis of Individual α-Synuclein Oligomers. *Angew. Chemie - Int. Ed.* **57**, 4886–4890 (2018).
19. Fusco, G. *et al.* Structural basis of membrane disruption and cellular toxicity by α-synuclein oligomers. *Science.* **358**, 1440–1443 (2017).
20. Ludtmann, M. H. R. *et al.* α-synuclein oligomers interact with ATP synthase and open the permeability transition pore in Parkinson's disease. *Nat. Commun.* **9**, 2293 (2018).
21. Outeiro, T. F. *et al.* Formation of toxic oligomeric α-synuclein species in living cells. *PLoS One* **3**, 1–9 (2008).
22. Flagmeier, P. *et al.* Ultrasensitive Measurement of Ca2+ Influx into Lipid Vesicles Induced by Protein Aggregates. *Angew. Chemie - Int. Ed.* **56**, 7750–7754 (2017).
23. Whiten, D. R. *et al.* Single-Molecule Characterization of the Interactions between Extracellular Chaperones and Toxic α-Synuclein Oligomers. *Cell Rep.* **23**, 3492–3500 (2018).
24. Mannini, B. *et al.* Stabilization and Characterization of Cytotoxic Aβ 40 Oligomers Isolated from an Aggregation Reaction in the Presence of Zinc Ions. *ACS Chem. Neurosci.* **9**, 2959–2971 (2018).
25. De, S. *et al.* Different soluble aggregates of Aβ42 can give rise to cellular toxicity through different mechanisms. *Nat. Commun.* **10**, (2019).
26. Esteras, N. *et al.* Insoluble tau aggregates induce neuronal death through modification of membrane ion conductance, activation of voltage-gated calcium channels and NADPH oxidase. *FEBS J.* 1–15 (2020) doi:10.1111/febs.15340.
27. De, S. *et al.* Soluble aggregates present in cerebrospinal fluid change in size and mechanism of toxicity during Alzheimer's disease progression. *Acta Neuropathol. Commun.* **7**, 113–120 (2019).
28. Kumar, S. T., Donzelli, S., Chiki, A., Syed, M. M. K. & Lashuel, H. A. A simple, versatile and robust centrifugation-based filtration protocol for the isolation and quantification of α-synuclein monomers, oligomers and fibrils: Towards improving experimental reproducibility in α-synuclein research. *J. Neurochem.* **153**, 103–119 (2020).
29. Iadanza, M. G., Jackson, M. P., Hewitt, E. W., Ranson, N. A. & Radford, S. E. A new era for understanding amyloid structures and disease. *Nat. Rev. Mol. Cell Biol.* **19**, 755–773 (2018).
30. MD, D. B. M. *et al.* a-Synuclein and tau concentrations in cerebrospinal fluid of patients presenting with parkinsonism: a cohort study. *Lancet Neurol.* **10**, 230–240 (2011).
31. Vaikath, N. N. *et al.* Antibodies against alpha-synuclein: tools and therapies. *J. Neurochem.*

150, 612–625 (2019).

32. Mitkevich, O. V. *et al.* DNA aptamers detecting generic amyloid epitopes. *Prion* **6**, 400–406 (2012).
33. Rahimi, F. Aptamers selected for recognizing amyloid β-protein—a case for cautious optimism. *Int. J. Mol. Sci.* **19**, 1–20 (2018).
34. Bondarev, S. A., Antonets, K. S., Kajava, A. V., Nizhnikov, A. A. & Zhouravleva, G. A. Protein co-aggregation related to amyloids: Methods of investigation, diversity, and classification. *Int. J. Mol. Sci.* **19**, 1–30 (2018).
35. Juhl, D. W. *et al.* Conservation of the Amyloid Interactome Across Diverse Fibrillar Structures. *Sci. Rep.* **9**, 1–14 (2019).
36. Voropai, E. S. *et al.* Spectral properties of thioflavin T and its complexes with amyloid fibrils. *J. Appl. Spectrosc.* **70**, 868–874 (2003).
37. Biancalana, M. & Koide, S. Molecular mechanism of Thioflavin-T binding to amyloid fibrils. *Biochim. Biophys. Acta - Proteins Proteomics* **1804**, 1405–1412 (2010).
38. Klunk, W. E. *et al.* Uncharged thioflavin-T derivatives bind to amyloid-beta protein with high affinity and readily enter the brain. *Life Sci.* **69**, 1471–1484 (2001).
39. Wu, C., Bowers, M. T. & Shea, J.-E. On the Origin of the Stronger Binding of PIB over Thioflavin T to Protofibrils of the Alzheimer Amyloid-β Peptide: A Molecular Dynamics Study. *Biophysj* **100**, 1316–1324 (2011).
40. Cho, H. J., Huynh, T. T., Rogers, B. E. & Mirica, L. M. Design of a multivalent bifunctional chelator for diagnostic 64Cu PET imaging in Alzheimer's disease. *Proc. Natl. Acad. Sci. U. S. A.* **117**, 30928–30933 (2020).
41. Qin, L., Vastl, J. & Gao, J. Highly sensitive amyloid detection enabled by thioflavin T dimers. *Mol. Biosyst.* **6**, 1791–1795 (2010).
42. Horrocks, M. H. *et al.* Single-Molecule Imaging of Individual Amyloid Protein Aggregates in Human Biofluids. *ACS Chem. Neurosci.* **7**, 399–406 (2016).
43. Ye, L. *et al.* In vitro high affinity α-synuclein binding sites for the amyloid imaging agent PIB are not matched by binding to Lewy bodies in postmortem human brain. *J. Neurochem.* **105**, 1428–1437 (2008).
44. Sulatskaya, A. I. *et al.* Investigation of α-synuclein amyloid fibrils using the fluorescent probe thioflavin T. *Int. J. Mol. Sci.* **19**, (2018).
45. De, S. *et al.* Different soluble aggregates of Aβ42 can give rise to cellular toxicity through different mechanisms. *Nat. Commun.* **10**, 1511–1541 (2019).
46. Xiong, F., Ge, W. & Ma, C. Quantitative proteomics reveals distinct composition of amyloid plaques in Alzheimer's disease. *Alzheimer's Dement.* 1–12 (2018).

47. Heywood, W. E. *et al.* Identification of novel CSF biomarkers for neurodegeneration and their validation by a high-throughput multiplexed targeted proteomic assay. *Mol. Neurodegener.* 1–16 (2015).
48. Guldbrandsen, A. *et al.* In-depth characterization of the cerebrospinal fluid (CSF) proteome displayed through the CSF proteome resource (CSF-PR). *Mol. Cell. Proteomics* **13**, 3152–3163 (2014).
49. Walsh, I., Seno, F., Tosatto, S. C. E. & Trovato, A. PASTA 2.0: An improved server for protein aggregation prediction. *Nucleic Acids Res.* **42**, 301–307 (2014).
50. Niu, M., Li, Y., Wang, C. & Han, K. RFAmyloid: A web server for predicting amyloid proteins. *Int. J. Mol. Sci.* **19**, (2018).
51. Mair, A., Xu, S. L., Branon, T. C., Ting, A. Y. & Bergmann, D. C. Proximity labeling of protein complexes and cell type-specific organellar proteomes in Arabidopsis enabled by TurboID. *bioRxiv* 1–45 (2019) doi:10.1101/629675.
52. Sousa, M. M. L., Steen, K. W., Hagen, L. & Slupphaug, G. Antibody cross-linking and target elution protocols used for immunoprecipitation significantly modulate signal-to noise ratio in downstream 2D-PAGE analysis. *Proteome Sci.* **9**, 45 (2011).
53. Kim, K., Lee, S., Ryu, S. & Han, D. Efficient isolation and elution of cellular proteins using aptamer-mediated protein precipitation assay. *Biochem. Biophys. Res. Commun.* **448**, 114–119 (2014).
54. Selkoe, D. J. The molecular pathology of Alzheimer's disease. *Neuron* **6**, 487–498 (1991).
55. Bruggink, K. A., Müller, M., Kuiperij, H. B. & Verbeek, M. M. Methods for analysis of amyloid-β aggregates. *J. Alzheimer's Dis.* **28**, 735–758 (2012).
56. Schuster, J. & Funke, S. A. Methods for the Specific Detection and Quantitation of Amyloid-β Oligomers in Cerebrospinal Fluid. *J. Alzheimer's Dis.* **53**, 53–67 (2016).
57. Soto, C. & Pritzkow, S. Protein misfolding, aggregation, and conformational strains in neurodegenerative diseases. *Nat. Neurosci.* **21**, 1332–1340 (2018).
58. Strømland, Ø., Kakubec, M. & Halskau, Ø. Detection of mis-folded protein aggregates from a clinical perspective. *J. Clin. Transl. Res.* **1**, 11–26 (2016).
59. Blennow, K. Cerebrospinal fluid protein biomarkers for Alzheimer's disease. *NeuroRX* **1**, 213–225 (2004).
60. Klunk, W. E. *et al.* Imaging Brain Amyloid in Alzheimer's Disease with Pittsburgh Compound-B. *Ann. Neurol.* **55**, 306–319 (2004).
61. Mintun, M. A. *et al.* [11C]PIB in a nondemented population. *Neurology* **67**, 446–452 (2006).
62. Kramer, R. H. & Karpen, J. W. Spanning binding sites on allosteric proteins with polymer-

linked ligand dimers. *Nature* **395**, 710–713 (1998).

63. Liang, J. *et al.* Dimerization of α-Conotoxins as a Strategy to Enhance the Inhibition of the Human α7 and α9α10 Nicotinic Acetylcholine Receptors. *J. Med. Chem.* **63**, 2974–2985 (2020).
64. Hühmer, A. F., Biringer, R. G., Amato, H., Fonteh, A. N. & Harrington, M. G. Protein analysis in human cerebrospinal fluid: Physiological aspects, current progress and future challenges. *Dis. Markers* **22**, 3–26 (2006).
65. Fusco, G. *et al.* Structural basis of membrane disruption and cellular toxicity by α-synuclein oligomers. *Science.* **358**, 1440–1443 (2017).
66. Gu, X. *et al.* Molecular modeling and affinity determination of scFv antibody: Proper linker peptide enhances its activity. *Ann. Biomed. Eng.* **38**, 537–549 (2010).
67. Silacci, M. *et al.* Linker length matters, Fynomer-Fc fusion with an optimized linker displaying picomolar IL-17A inhibition potency. *J. Biol. Chem.* **289**, 14392–14398 (2014).
68. Wang, W., Singh, S., Zeng, D. L., King, K. & Nema, S. Antibody Structure, Instability, and Formulation. *J. Pharm. Sci.* **96**, 1–26 (2007).
69. Zheng, S. *et al.* Investigating the Degradation Behaviors of a Therapeutic Monoclonal Antibody Associated with pH and Buffer Species. *AAPS PharmSciTech* **18**, 42–48 (2017).
70. Le Basle, Y., Chennell, P., Tokhadze, N., Astier, A. & Sautou, V. Physicochemical Stability of Monoclonal Antibodies: A Review. *J. Pharm. Sci.* **109**, 169–190 (2020).
71. Savage, M. J. *et al.* A sensitive Aβ oligomer assay discriminates Alzheimer's and aged control cerebrospinal fluid. *J. Neurosci.* **34**, 2884–2897 (2014).
72. Sengupta, U. *et al.* Tau oligomers in cerebrospinal fluid in Alzheimer's disease. *Ann. Clin. Transl. Neurol.* **4**, 226–235 (2017).
73. Kolarova, M., Sengupta, U., Bartos, A., Ricny, J. & Kayed, R. Tau Oligomers in Sera of Patients with Alzheimer's Disease and Aged Controls. *J. Alzheimer's Dis.* **58**, 471–478 (2017).
74. Hansson, O. *et al.* Levels of cerebrospinal fluid α-synuclein oligomers are increased in Parkinson's disease with dementia and dementia with Lewy bodies compared to Alzheimer's disease. *Alzheimer's Res. Ther.* **6**, 4–9 (2014).

Methods

This research complies with all relevant ethical regulations and was approved by the Ethics Committee at University of Gothenburg (EPN 140811).

Synthesis of N-biotinylated bis-benzothiazole*: *CAP-1

(**A**) ***bis*-Mesylate**:

To a solution of *diol* (1.47 g, 5.0 mmol, 1.0 equiv.) in anhydrous CH_2Cl_2 (10 mL) was added Et_3N (2.53 mL, 18.0 mmol, 3.6 equiv) at 0°C. A solution of methanesulfonyl chloride (1.01 mL, 13.0 mmol, 2.6 equiv.) in CH_2Cl_2 (5 mL) was then added dropwise. The reaction was allowed to warm to room temperature (rt) and stirred for an additional 18 h. Aqueous hydrochloric acid (1 N, 100 mL) was added slowly and the reaction mixture extracted with CH_2Cl_2 (4 × 60 mL). The combined organic layers were washed with saturated sodium bicarbonate solution (50 mL) and brine (60 mL), dried over Na_2SO_4, and concentrated under reduced pressure to give the *bis*-mesylate **(A)** (1.57 g, 3.50 mmol, 70%) as a colourless oil.

(**B) Boc-protected *bis*-benzothiazole**:

Sodium hydride (60% in oil, 19 mg, 0.44 mmol, 2.2 equiv) was added in one portion to a solution of 2-(4-(dimethylamino)phenyl)benzo[*d*]thiazol-6-ol (110 mg, 0.4 mmol, 2.0 equiv) in DMF (5 mL) at rt. The suspension was stirred for 1 h giving a colourless solution to which the *bis*-mesylate (**A**) (90 mg, 0.2 mmol, 1.0 equiv) was added then heated to 80°C for 18 h. After cooling to rt, H_2O (15 mL) was added with vigorous stirring. The resulting precipitate was collected by filtration, washed with water (10 mL) and ethanol (10 mL) to give the Boc-protected *bis*-benzothiazole **(B)** (64 mg 0.08 mmol, 40%) as white solid. m.p.: 122–124°C.

(C) NH *bis*-benzothiazole:

Boc-protected *bis*-benzothiazole (**B)** (64 mg 0.08 mmol, 1 equiv.) was added to a solution of HCl (4 M in MeOH, 3 mL) at rt. After 1 h, aqueous NaOH (3 M, 10 mL) and EtOAc (10 mL) were added and the layers separated. The aqueous layer was further extracted with EtOAc (2 × 10 mL) and the combined organic layers dried over Na_2SO_4 and concentrated to give the NH *bis*-benzothiazole **(C)** (55 mg, 80 mmol, 99%) as light yellow solid. m.p.: 168–170 °C.

(D) **N-Biotinylated *bis*-benzothiazole:**

To a solution of biotin (49 mg, 0.2 mmol, 1 equiv) in anhydrous DMF (2 mL) was added *i*Pr_2NEt (452 μL, 0.26 mmol, 1.3 equiv) and benzotriazol-1-yl-oxytripyrrolidinophosphonium

hexafluorophhosphate (PyBOP, 135 mg, 0.26 mmol, 1.3 equiv). After 30 min, the amine **C** (140 mg, 0.2 mmol, 1 equiv) and *i*Pr_2NEt (350 μL, 1.0 equiv) in anhydrous DMF (1 mL) was added dropwise. After 18 h, saturated NH_4Cl (10 mL) was added and the mixture extracted with EtOAc (3 × 5 mL). The combined organic layers were washed with brine (10 mL), dried over Na_2SO_4 and concentrated under reduced pressure. The residue was purified by column chromatography [SiO_2, Methanol–CH_2Cl_2, 1:8] to give **N-biotinylated *bis*-benzothiazole (CAP-1) (D)** (56 mg, 0.06 mmol, 30%) as a light yellow solid. m.p.: 120–122°C.

Aggregation of α-synuclein

Monomeric wild-type α-synuclein was purified from *Escherichia coli* as previously described[75].
Prior to use, α-synuclein aliquots were ultracentrifuged at 350000 *g* during 1h at 4°C using TL120.2 rotor (Beckman) in an Optima TLX Ultracentrifuge (Beckman) to remove possible seed contaminants. 2/3 of the total volume in the tube was used as the supernatant fraction (monomers only) and removed with minimal perturbation to avoid remixing of unwanted seeds. Afterwards, the protein concentration was determined using a nanodrop ($\varepsilon^{275\ nm}$ (Tyr) 5600 $M^{-1}cm^{-1}$) and then the α-synuclein was diluted in cold Tris buffer 25 mM supplemented with NaCl 100 mM, pH 7.4 and 0.01% NaN_3 (to prevent bacterial growth) to a final concentration of 70 μM. This solution was incubated in the dark at 37°C with constant agitation at 200 rpm (New Brunswick Scientific Innova 43) and aliquots were taken at desired times (0 h monomers, 6-8 h oligomers and 1-5 d for mature fibrils). All time points were imaged on TIRFM setup before any experiment to confirm the presence/absence of the desired α-synuclein intermediate species *i.e* absence of aggregates at t 0 h and fibrils on 6 to 8 h and presence of diffracted limited size aggregates on the 6 to 8 h time point aliquots. All steps were carried out using LoBind microcentrifuge tubes (Eppendorf, Hamburg, Germany) to limit surface adsorption. For binding affinity experiments and pulldown (Figure 2d) mature α-synuclein fibrils (5 days incubation) were sonicated with a probe sonicator (Bandelin, Sonopuls HD 20170), 4 times of 15 s at 10% power and the tube was placed on a beaker containing ice to minimise overheating effects on the tube walls, afterwards the protein was aliquoted and stored at -80°C until use.

Preparation and photophysical characterization of CAP-1

CAP-1 1 mM stock solution was prepared in DMSO, divided into 20 μL aliquots and stored at -20°C. Aliquots were used once to avoid freeze and thaw cycles. The photophysical properties of CAP- 1 were determined using a Varian Cary Eclipse fluorescence spectrophotometer (Mulgrave, Australia). Experimental settings used were λ_{ex} = 355 nm (5 - 10 nm bandwidth), λ_{em} = 370-600 nm (5 - 10 nm bandwidth). UV–vis absorption and fluorescence (both excitation and emission) spectral

characterization of CAP-1 (20 μM) were carried out in both PBS and Tris 25 mM supplemented with NaCl 100 mM, pH 7.4. To test CAP-1 solubility in PBS, different dilutions were prepared between 0 nM and 200 nM and the emission spectrum recorded using λ_{ex} = 355 nm. Data point were plotted as $[CAP\text{-}1]_{PBS}$ *vs.* maximum fluorescence intensity. The linear relationship between concentration and fluorescence intensity (R^2 =0.98) strongly suggests CAP-1 obeys the Beer-Lambert law and is therefore completely soluble in the range used.

Measurement of protein aggregation in plate reader

Fluorescence kinetics measurements of α-synuclein with either CAP-1 or ThT were monitored using a FLUOstar® Omega fluorescence plate reader (BMG Labtech, Aylesbury, UK) in bottom reading mode under quiescent conditions. Corning 96-well plates with half-area (3881, polystyrene, black with clear bottom) non-binding surfaces sealed with aluminium sealing tape were used for each experiment. Monomeric α-synuclein 40 μM (+ 2.4 μM preformed fibrils) was incubated in the presence of 50 μM CAP-1 or ThT at 37°C under quiescent conditions for 4 days with data point collection every 6 min[76].

α-synuclein preparation for plate reader measurements

Monomeric α-synuclein was prepared from purified α-synuclein subjected to gel filtration using a Superdex 75 10/300 GL column (Cytiva Life Sciences) equilibrated in MES buffer (10 mM 2-(N-morpholino) ethanesulfonic acid, 1 mM EDTA, pH 5.5), and the peak corresponding to monomeric α-synuclein peptide was collected in a low-binding test tube (Corning) on ice. Seed fibrils were produced as described previously[76]. Briefly, concentrated stock α-synuclein monomer (100-200 μM) was incubated at 40 °C for 72 hours with a Teflon bar on an RCT Basic Heat Plate (IKA, Staufen, Germany) in PBS. To estimate the fibril concentration (monomeric equivalent) the solution was centrifuged at 21130 *g* in a benchtop centrifuge (Eppendorf). The concentration of the remaining α-synuclein monomer in the supernatant was estimated by absorbance using a NanoDrop 2000 (Thermo Fisher Scientific) and was subtracted from the concentration at the start of the aggregation. The volume of the supernatant was subsequently replaced by MES buffer and the stock was aliquoted and stored at -80°C. To prepare α-synuclein seeds, the fibril stock was diluted to 5 μM final concentration in protein low binding tubes and sonicated for 15 s (1 s on, 1 s off) using a probe sonicator.

Binding affinity

The binding affinity measurements were conducted on a Duetta™ spectrofluorometer (HORIBA) and the experimental settings used for CAP-1 and S1 (monovalent version of CAP-1) were λ_{ex} =

355 nm (10 nm bandwidth), λ_{em} = 370-600 nm (10 nm bandwidth) and for ThT λ_{ex} = 440 nm (10 nm bandwidth), λ_{em} = 455-600 nm (10 nm bandwidth). Sonicated α-synuclein (200 nm, see SI.14) was prepared as described above and $A\beta_{40}$ fibrils were obtained by incubating 4 μM of monomeric $A\beta_{40}$ in PBS for 4 h at 37°C with constant agitation followed by same sonication procedure. Different concentrations of dye (CAP-1 and S1 up to 200 nM and ThT up to 10 μM) were incubated with 100 nM of either α-synuclein or $A\beta_{40,}$ for 20 min before measurement in PBS. The K_d for ThT was obtained by fitting the experimental points to a hyperbolic curve (specific binding). Since CAP-1 and S1 are fluorescent in the absence of binding to aggregates, an equivalent set of data points was also collected in the absence of protein (dye only curve). A model that takes account of the change in fluorescence between bound and unbound molecule was then used (see ref[77-79] and supplementary information Methods). This is important for CAP-1 and S1 since there is only a small increase in fluorescence on binding fibrils.

Amyloid precipitation assay – AP

The amyloid precipitation (AP) assay consists of the pulldown of protein aggregates (*e.g.* α-synuclein) using streptavidin-Dynabeads (MyOne™ Streptavidin C1, Invitrogen) conjugated with CAP-1. Briefly, 30 μL of beads/sample were removed from the vial, resuspended in 1 mL PBS and placed on a magnet for 2-3 min for separation and the supernatant discarded (this step was repeated three times). Afterwards, the beads were resuspended in 1 mL of CAP-1 30 μM and the tube placed in a revolver mixer for incubation at room temperature during 1h. Following, the tube was placed on the magnet for 2-3 min and the supernatant discarded. The beads were washed three times with PBS as before. Finally, the beads were resuspended in 500 μL solution containing α-synuclein 10 μM (monomers alone, or mixture of aggregates) and left in the revolver mix for 2h or overnight at 4°C. In the end, the tube was placed on the magnet for 2 to 3 min and 450 μL of supernatant were removed to a clean tube and labelled as 'depleted' fraction, both the depleted fraction and the 'beads' were kept at 4°C until use. All steps were carried out in LoBind microcentrifuge tubes (Eppendorf, Hamburg, Germany) to limit surface adsorption.

Detection of bead-bound α-synuclein

After amyloid precipitation (AP) both 'beads' (diluted 1:32 in PBS) and the 'depleted' fraction were added to a 96-well half-area plate with clear bottom (Corning 3881, Kennebuck ME, USA) for bulk fluorescence measurement. The plate was placed in a plate reader (CLARIOstar; BMG Labtech, Ortenberg, Germany) and Fluorescence intensity (bottom reading) was measured straight away at room temperature using the following settings: end-point mode, 440-10/480-10 nm excitation and

emission wavelengths respectively; or spectrum mode, excitation at 355 nm and emission from 380-600 nm.

Preparation of slides for single-molecule measurements

Borosilicate glass coverslips (VWR international, 20 × 20 mm, product number 631-0122) were cleaned using an argon plasma cleaner (PDC-002, Harrick Plasma) for 1 h to remove impurities and contaminants and create a hydrophilic surface. Frame-seal slide chambers (9 ×9 mm^2, Biorad, Hercules, CA, product number SLF-0601) were affixed to the glass, and 50 μL of poly-L-lysine (70000-150000 molecular weight, Sigma-Aldrich, product number P4707-50 ML) was added to the coverslip on the inside of the chamber and incubated for 30 min before being washed with filtered PBS buffer (Whatman Anatop 25 0.02 μm). Each batch of coverslips was tested for fluorescent artefacts (*i.e.* false positives) by imaging thioflavin T (ThT) 5 μM. ThT stock solution was prepared as described elsewhere[80] and ThT working solution (50-100 μM) was filtered (Whatman Anatop 25 0.02 μm) prior to use and concentration determined using $\varepsilon^{412\ nm}$ 36000 $M^{-1}cm^{-1}$.

Total internal reflection fluorescence microscopy (TIRFM) imaging

Imaging was performed using a homebuilt total internal reflection fluorescence microscope as reported previously[80]. Briefly, this imaging mode restricts detectable axial fluorescence signal to within ~200 nm from the glass-water interface. For imaging of recombinant α-synuclein or cerebrospinal fluid (CSF) in the presence of ThT or CAP-1, the output from laser operating at 405 nm (Oxxius LaserBoxx, product number LBX-405-100-CIR-PP) was aligned and directed parallel to the optical axis at the edge of a 60× Plan Apo TIRF, NA 1.45 oil objective, (Nikon Corporation), mounted an Eclipse TE2000-U microscope (Nikon Corporation) fitted with a Perfect Focus unit. Fluorescence was collected by the same objective and was separated from the returning TIR beam by a dichroic (Di01-R405/488/561/635, Semrock), and passed through appropriate filter (FF01-480/40-25 or FF01-434/17-25 Semrock, for ThT or CAP-1, respectively). The images were recorded on an EMCCD camera (Evolve 512, Photometrics) operating in frame transfer mode (EMGain of 6.5 e−/ADU and 250 ADU/photon). Each pixel was 241 nm in size. For each data set, 4×4 image grids were measured in at least three different regions of the coverslip. The distance between the nine images measured in each grid was set to 350 μm, and was automated (bean-shell script, Micromanager) to prevent user bias. Images were recorded at 50 ms exposure time for 100 frames with 405 nm illumination (150–200 W/ c2).

Recombinant α-synuclein and CSF were diluted in filtered PBS (Whatman Anatop 25 0.02 μm) and mixed with ThT or CAP-1 for a final imaging volume of 50 μL. The ThT and CAP-1 imaging

concentration was 5 μM while the α-synuclein concentration changed between experiments (1 μM for sonicated fibrils, 2.8 μM for comparison of time points, and 7 μM for t=8h). For CSF samples, we used 15 μL of neat CSF and 24 μL of depleted fraction AP. All samples were stored and diluted in LoBind microcentrifuge (Eppendorf, Hamburg, Germany) to limit surface adsorption. For imaging the beads (Figure 2 c) we used 1 μL of 'beads' fraction (50 μL in total) in 49 μL of PBS.

AP of α-synuclein spiked in CSF followed by on-bead digestion

The CSF sample aliquots used were de-identified leftover aliquots from clinical routine analyses, following a procedure approved by the Ethics Committee at University of Gothenburg (EPN 140811). Amyloid precipitation was carried out as described above, except for using 50 μL of beads per sample instead of 30 μL. After conjugation with CAP-1 and washing the beads were resuspended in a solution containing 600 μL of CSF and 400 μL PBS. α-synuclein was spiked into the CSF, adding either monomer alone or a mixture containing monomers and oligomers (previously characterized using TIRFM). Concentrations spiked were 1 pM, 100 pM, 1 nM, 10 nM and 100 nM and samples were prepared in triplicate. The immunoprecipitation method for CSF samples was performed according to Bhattacharjee *et al.* 2019 with minor modifications[81-82]. Briefly, after overnight incubation at 4°C the KingFisher magnetic particle processor (Thermo Fisher Scientific) was used to wash and resuspend the beads. The beads were first extracted, then washed two times with PBS, one time with 1 mL of 50 mM ammonium bicarbonate (NH_4HCO_3, pH 8.0; Sigma-Aldrich) and finally resuspended in 100 μL of 50 mM NH_4HCO_3 for on-bead digestion. For on-bead digestion 10 μL of 10 mM 1,4-dithiothreitol (DTT) in NH_4HCO_3 was added to the solution, vortexed and incubated for 30 min at 60°C and, then cooled down to room temperature for 15 min. Afterwards, 10 μL of 10 mM iodoacetamide (IAM) in NH_4HCO_3 was added, vortexed and incubated for 30 min at 25°C in darkness. Finally, 10 μL of trypsin 5 ng/μL in NH_4HCO_3 was added, vortexed and incubated at 37ºC overnight with shaking at 400 rpm. The reaction was stopped by addition of 10 μL 10% formic acid (FA). Finally, samples were centrifuged at 16910 *g* for 10 min, 4°C and the supernatant collected in a different vial. The magnetic beads were washed with 50 μL NH_4HCO_3, then centrifuged again and the supernatant was collected in the same vial as before. Then collected supernatants were dried by speedvac.

LC-MS/MS of α-synuclein

High-resolution parallel reaction monitoring (PRM) analyses were performed on a quadrupole–orbitrap mass spectrometer Q-Exactive (Thermo Fisher Scientific) coupled to an Ultimate 3000 chromatography system (Thermo Fisher Scientific). Mobile phases were 0.1% aqueous FA(v/v) (A) and 0.1% FA in 84% ACN in water (v/v) (B). The mixture of Heavy-isotope-labeled peptide

standards of α-synuclein (Heavy Peptide FasTrack 1 standards, ThermoFisher Scientific, USA) was prepared in 20% ACN containing 0.1% FA as follows: α-syn$_{13-21}$, α-syn$_{35-43}$, α-syn$_{46-58}$, α-syn$_{61-80}$, and α-syn$_{81-96}$ (10 fmoles/µL each). Then the dried samples after pull down and on-bead digestion were dissolved in 20 µl of mixture of heavy-isotope-labelled (IS) peptide standards for 1 h and then transferred to LC vials for analysis. Samples were loaded directly onto a HypersilGold-C18 column, (length 100 mm, inner diameter 2 mm, particle size 1.9 µm, Thermo Fischer Scientific) with 0.1% aqueous FA at 300 µL/min. After 2 min of loading, the peptides were eluted off the column using the following linear gradient steps: 0 min 0%B; 4 min 17%B; 16 min 35%B; 17.5 min 100%B; 20 min 0%B. The global MS parameters were: positive ion mode; spray voltage 3.5 kV; vaporizer temperature +350°C; sheath gas pressure 40 psi; auxiliary gas pressure 25 arbitrary units; capillary temperature +350°C; collision gas pressure 1.9 mTorr. The instrument was set to acquire scheduled pairs or triplets of PRM scans and subsequent all ion fragmentation scans allowing simultaneous detection of both the α-synuclein peptide and the corresponding IS peptide standards. The settings were common for both scans types and were as follows: resolution, 70,000; AGC target, 3e6; maximum injection time, 250 ms; isolation window, 3.0 m/z and normalized collision energy 35. Data acquisition and analysis were performed with Xcalibur software version 2.2 SP1.48 (ThermoFisher Scientific) and Pinpoint 1.3.0 (ThermoFisher Scientific) for determining selected fragment ion peak areas, respectively. The MS accuracy was ± 10 ppm centred at 0, a MS/MS accuracy of ± 15 ppm and the isolation mode set to MS/MS with an isolation width of 3.0 u. The peaks were detected using a chromatographic peak with a window size of ± 2.0 min. The complete peak area was determined after using four points of smoothing. The scheduling window size for identified transitions was ± 0.5 min. The detected fragment ion peaks were manually inspected for accuracy and absence of interferences from other peptides than the peptide of interest, including fragments originating from other product ions in the same pair/triplet. The relative amount of spiked unlabelled or 15N-labeled α-synuclein peptide was calculated by normalizing the measured peak area with the peak area of the corresponding IS peptide.

Database search parameters

Specified search parameters: database (Swiss-Prot), taxonomy (*Homo sapiens*), enzyme (trypsin), variable modifications (acetyl [N-term] and oxidation [M]), static modification (carbamidomethyl [C]), mass values (monoisotopic), peptide mass tolerance (± 10 ppm), fragment mass tolerance (± 10 mmu), and maximum 2 missed cleavages. On average, individual ions scores > 40 indicate identity or extensive homology ($P < 0.05$) was considered for identification. Ions score is -10log(P), where P is the probability that the observed match is a random event.

Membrane permeability assay

Details of this method have been described previously[83]. Studies have shown that single vesicle assay can be used to measure the toxicity of β-sheet rich protein aggregates present in CSF[84] or complex biological mixture[85]. See supplementary materials for details

Data analysis

Microscopy images were analysed using ImageJ and Matlab. GraphPad Prism 9 was used for statistical analysis, plotting and curve fitting. Statistical analysis was performed using unpaired two-tailed Student's t test to analyse differences between two groups, or a one-way ANOVA and Tukey's *post hoc* comparison to analyse differences among three or more groups. Differences were considered to be statistically significant if $p < 0.05$. To determine the number of fluorescent puncta in each image an average of the entire stack was generated and used to detect each protein aggregate using the Find Maxima function in ImageJ (with a threshold value of 180 Figure 2e). To compare proteins pulled down from control (A) and PD (B) CSF in the presence (1) and absence (2) of CAP-1 we used a custom Matlab code (available on request). From the original database search (Swiss-Prot) we generated new data sets for each condition (A1, A2, B1 and B2) based on 2 criteria: proteins present in all three replicates and with at least 2 unique peptides. Then we compared list A1 with A2 and B1 with B2. See SI Table 3 – 8 for results: List of common proteins (Table 3 (A1-A2) and Table 6 (B1-B2)) and list of exclusive proteins (Table 4 (A1), Table 5 (A2), Table 7 (B1) and Table 8 (B2). Finally, we used PASTA 2.0[86] (Table 1-8) and RFAmyloid[87] (Table 9), two bioinformatic tools to predict % of α-helix and % of β-strand, and amyloid formation, from protein sequence analysis, respectively.

Data Availability

The data supporting the findings of this study are available within the paper and its Supplementary Information and are also available from the corresponding authors on reasonable request. We used Swiss-Prot database to identify the proteins presents in the mass spectrometry samples.

Code Availability

The custom Matlab code used for analysis of the proteins is available on GitHub.

References for Methods

75. Hoyer, W. *et al.* Dependence of α-synuclein aggregate morphology on solution conditions. *J. Mol. Biol.* **322**, 383–393 (2002).
76. Arosio, P., Vendruscolo, M., Dobson, C. M. & Knowles, T. P. J. Chemical kinetics for drug discovery to combat protein aggregation diseases. *Trends Pharmacol. Sci.* **35**, 127–135 (2014).
77. Stein, R. A., Wilkinson, J. C., Guyer, C. A. & Staros, J. V. An analytical approach to the measurement of equilibrium binding constants: Application to EGF binding to EGF receptors in intact cells measured by flow cytometry. *Biochemistry* **40**, 6142–6154 (2001).
78. Breen, C. J., Raverdeau, M. & Voorheis, H. P. Development of a quantitative fluorescence-based ligand-binding assay. *Sci. Rep.* **6**, 1–9 (2016).
79. GraphPad. Fitting binding of fluorescent ligands. *KNOWLEDGEBASE - ARTICLE #1725* https://www.graphpad.com/support/faq/fitting-binding-of-fluorescent-ligands/ (2011).
80. Horrocks, M. H. *et al.* Single-Molecule Imaging of Individual Amyloid Protein Aggregates in Human Biofluids. *ACS Chem. Neurosci.* **7**, 399–406 (2016).
81. Bhattacharjee, P. *et al.* Mass Spectrometric Analysis of Lewy Body-Enriched α-Synuclein in Parkinson's Disease. *J. Proteome Res.* **18**, 2109–2120 (2019).
82. Brinkmalm, A., Öhrfelt, A., Bhattacharjee, P. & Zetterberg, H. Detection of α-Synuclein in Biological Samples Using Mass Spectrometry BT - Alpha-Synuclein: Methods and Protocols. in *Alpha-Synuclein: Methods and Protocols* vol. 1948 (Springer New York, 2019).
83. Flagmeier, P. *et al.* Ultrasensitive Measurement of Ca2+ Influx into Lipid Vesicles Induced by Protein Aggregates. *Angew. Chemie - Int. Ed.* **56**, 7750–7754 (2017).
84. Drews, A. *et al.* Inhibiting the Ca2+ Influx Induced by Human CSF. *Cell Rep.* **21**, 3310–3316 (2017).
85. De, S. *et al.* Different soluble aggregates of Aβ42 can give rise to cellular toxicity through different mechanisms. *Nat. Commun.* **10**, (2019).
86. Walsh, I., Seno, F., Tosatto, S. C. E. & Trovato, A. PASTA 2.0: An improved server for protein aggregation prediction. *Nucleic Acids Res.* **42**, 301–307 (2014).
87. Niu, M., Li, Y., Wang, C. & Han, K. RFAmyloid: A web server for predicting amyloid proteins. *Int. J. Mol. Sci.* **19**, (2018).

Supplementary Information

Structure specific amyloid precipitation in biofluids

M. Rodrigues[1,2], P. Bhattacharjee [3,4], A. Brinkmalm[3,4], D. T. Do[5], C. M. Pearson[5], S. De[1,2,6], A. Ponjavic[1,7,8], J. A. Varela[1,9], K. Kulenkampff[1,2], I. Baudrexel[1], D. Emin[1,2], F. S. Ruggeri[1,10,11], J. E. Lee[1,12], A. R. Carr[1], T. P. J. Knowles[1], H. Zetterberg[3,4,13,14], T. N. Snaddon[5*], S. Gandhi[13,15*], S. F. Lee[1*] and D. Klenerman[1,2*]

[1] *Department of Chemistry, University of Cambridge, Lensfield Road, Cambridge, CB2 1EW, UK*

[2] *UK Dementia Research Institute, University of Cambridge, Cambridge, CB2 0XY, UK.*

[3] *Department of Psychiatry and Neurochemistry, Institute of Neuroscience and Physiology, the Sahlgrenska Academy at the University of Gothenburg, S-431 80 Mölndal, Sweden*

[4] *Clinical Neurochemistry Laboratory, Sahlgrenska University Hospital, Mölndal, Sweden*

[5] *Department of Chemistry, Indiana University, 800 E. Kirkwood Ave. Bloomington, IN 47405, USA.*

[6] *Sheffield Institute for Translational Neuroscience, University of Sheffield, Western Bank, Sheffield, S10 2TN, UK*

[7] *School of Physics and Astronomy, University of Leeds, Woodhouse, Leeds, LS2 9JT, UK*

[8] School of Food Science and Nutrition, University of Leeds, Woodhouse, Leeds, LS2 9JT, UK

[9] *School of Physics and Astronomy, University of St Andrews, North Haugh, St Andrews, KY16 9SS, UK*

[10] *Laboratory of Organic Chemistry, Wageningen University & Research, Stippeneng 4, 6703 WE, The Netherlands*

[11] *Physical Chemistry and Soft Matter, Wageningen University & Research, Stippeneng 4, 6703 WE, The Netherlands*

[12] *School of Chemistry, University of Edinburgh, Joseph Black Building, David Brewster Rd, Edinburgh, EH9 3FJ UK*

[13] *Department of Neurodegenerative Disease, UCL Institute of Neurology, London, WC1N 3BG, UK*

[14] *UK Dementia Research Institute at UCL, Gower Street, London, WC1E 6BT, UK*

[15] *The Francis Crick Institute, 1 Midland Road, King's Cross, London, NW1 1AT, UK*

* Joint corresponding authors

Supplementary Methods

Imaging of amyloid-β_{1-42} and tau fibrils

1 μM amyloid-β_{1-42} ($a\beta_{42}$) and 100 nM tau fibrils were imaged in similar way to α-synuclein. Prior to imagining protein aggregates were diluted in PBS and incubated with either 5 μM of ThT or CAP-1, or 50 nM of pFTAA (tau). $A\beta_{42}$ fibrils were obtained by incubating 4 μM of monomeric $a\beta_{42}$ (Stratech, Catalogue Number: A-1167-2-RPE) in PBS for 4h at 37°C with constant agitation. Tau aggregation reactions were performed using 50 μM 0N4R htau (InVivo BioTech Services GmbH, Germany) in buffer containing 100 mM Tris, 150 mM NaCl and 0.1 mM EDTA. The aggregation was initiated by the addition of 0.05 mg/ml heparin (1:4 heparin:tau ratio). The aggregation reaction was incubated at 37°C under quiescent conditions for 120 h before imaging.

Modelling of binding curve

The model used is included in GraphPad inbuilt equations and the constants are the concentration of the receptor (fibril binding sites) and the background (fluorescence without dye)[77-79]. The first step was to subtract the respective blank from each data set (dye only and dye+protein) and normalise by the molecular fluorescence (slope of dye only). The exact number of binding sites per fibril is difficult to determine but the upper limit is 25 nM, assuming 1 molecule of ThT binds to 4 molecules of α-synuclein[37]. The lower limit is 333 pM, assuming that there is just one binding site per fibril and estimating that the 200 nm long fibrils used in the experiment contain on average 300 monomers (based on a fibril diameter of 6 nm and the standard density of a folded protein of 1.35 kg l^{-1}). We tried a range of values between these limits and found that, as expected, this had little effect on the value K_d determined. Therefore, we decided to use the intermediate value of 3.33 nM to determine K_d.

Atomic Force Microscopy (AFM)

AFM was performed on freshly cleaved mica substrates. Aliquots (10 μL) of each diluted sample were deposited on the substrate at room temperature, incubated for 10 min, rinsed with 1 mL Milli Q water, and then dried under a gentle nitrogen flow. AFM maps were generated by means of a JPK nanowizard2 system (JPK Instruments, Germany) operating in tapping mode and equipped with a silicon tip (PPP-NCHR, 5 Nm^{-1}) with a nominal radius of <10 nm.

Electron microscopy

Electron microscopy images were acquired on a scanning electron microscopy with a retractable STEM detector (TESCAN MIRA3 FEG-SEM) using 30kv. Holey carbon grids (EM Resolutions,

300 mesh Copper) were glow-discharged for hydrophilization using Quorum Technologies GloQube Dual Chamber Glow Discharge System (25 mA, 60 sec, negative) and then 10 µL of α–synuclein samples (fibrils or sonicated fibrils) was added and let dry for 15 min (excess carefully removed with filter paper). Prior to imaging grids were plasma cleaned (Fischione Model 1070 Nanoclean Plasma Cleaner) using a 25% oxygen and 75% argon gas mixture to remove carbonaceous debris, for 15 sec.

Liposome assay

Briefly, Phospholipids 16:0-18:1 1-palmitoyl-2-oleoyl-glycero-3-phosphocholinePC (Avanti Polar Lipids) and biotinylated lipids 1-oleoyl-2-[12-biotinyl(aminododecanoyl)]-sn-glycero-3-phosphocholine18:1-12:0 Biotin PC (Avanti Polar Lipids) were mixed 100:1 ratio and dissolved in HEPES buffer (pH 6.5) with 100 µM Cal-520. Using dry ice and a water bath, five freeze-and-thaw cycles were performed to control the unilamellarity. Then the mixed lipid solution was passed 10 times through an extruder (Avanti Polar Lipids, A) with a membrane of 200 nm diameter. To remove the free dye from the surrounding solution containing dye-filled vesicles, size-exclusion chromatography was performed using Superdex 200. The size of the vesicles was confirmed using a zeta-sizer. The vesicles are immobilised using biotin-neutravidin linkage in glass coverslips. Before immobilisation of the vesicles, each coverslip is cleaned using argon based plasma cleaner and sample chambers were made by affixing Frame-Seal incubation chambers onto the glass slides. For homogeneous surface treatment, 50 µL of a mixture of 100:1 PLL-g-PEG and PLL-g-PEG biotin (both 1 g/L) in HEPES buffer (50 mM, pH 6.5) was added to the coverslip inside of the chamber and incubated for 30 min. Then the surface was washed with filtered HEPES buffer and a solution of NeutrAvidin (50 µL of 0.1 mg/mL in MilliQ) added and incubated for 15 min before being washed. 50 µL of vesicles was added to the coverslip and let to adsorb for 20 min before solution is removed and replaced by 30 µL of Ca^{2+} containing buffer solution Leibovitz's L-15 and background image was recorded ($F_{background}$). Thereafter, 16 µL of sample (16 µL of AP depleted fraction or 10 µL of neat CSF + 6 µL PBS) was added and incubated for 20 min and images were acquired (F_{sample}). Next, 10 µL of ionomycin solution added and same fields of view were acquired ($F_{ionomycin}$). For each field of view (10 to 15 in total) 50 images were taken with an exposure time of 50 ms. The relative Ca^{2+} influx into an individual vesicle due to protein aggregates present in CSF was then determined as

$$Ca^{2+}\text{influx} = \frac{F_{sample} - F_{background}}{F_{Ionomycin} - F_{background}}$$

The average degree of was calculated by averaging the Ca^{2+} influx into individual vesicles. The membrane permeabilization experiments were performed using a homebuilt TIRF imaging setup

microscope using 1.49 100× Nikon TIRF Objective. For excitation 488-nm laser (Toptica) beam and images were acquired using an air-cooled EMCCD camera (Evolve Delta).

Supplementary Figures

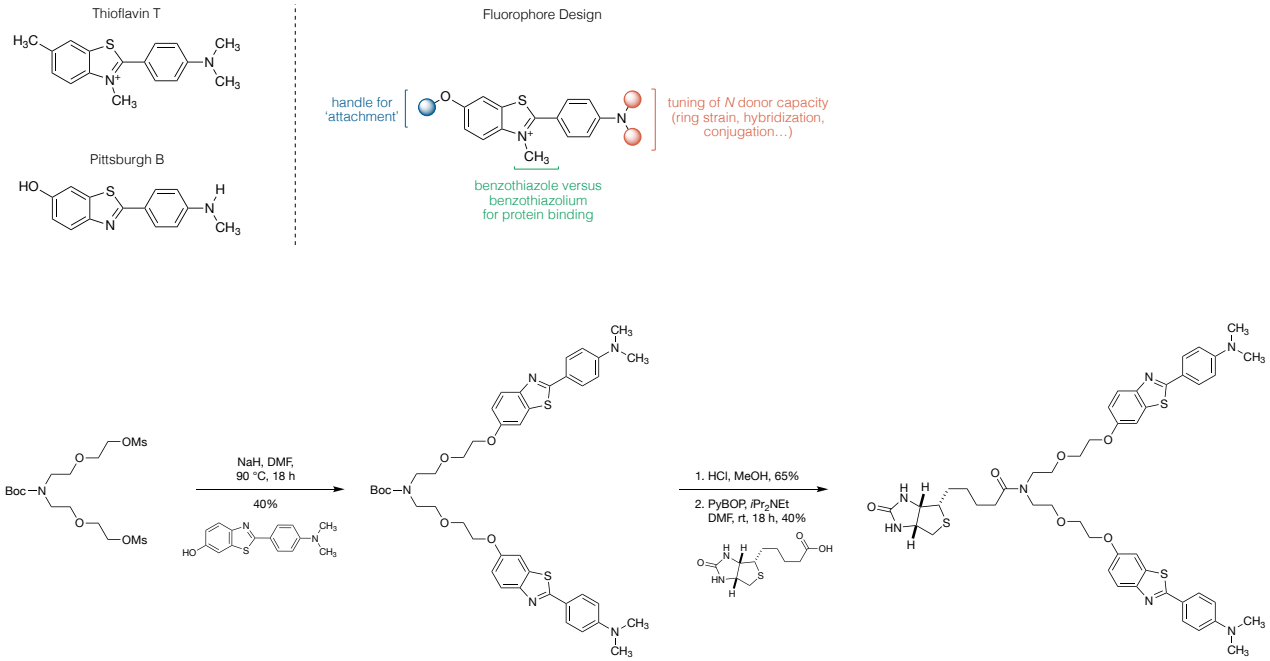

SI.1 - Rational design and characterization of CAP-1 and outline of CAP-1design and synthesis.

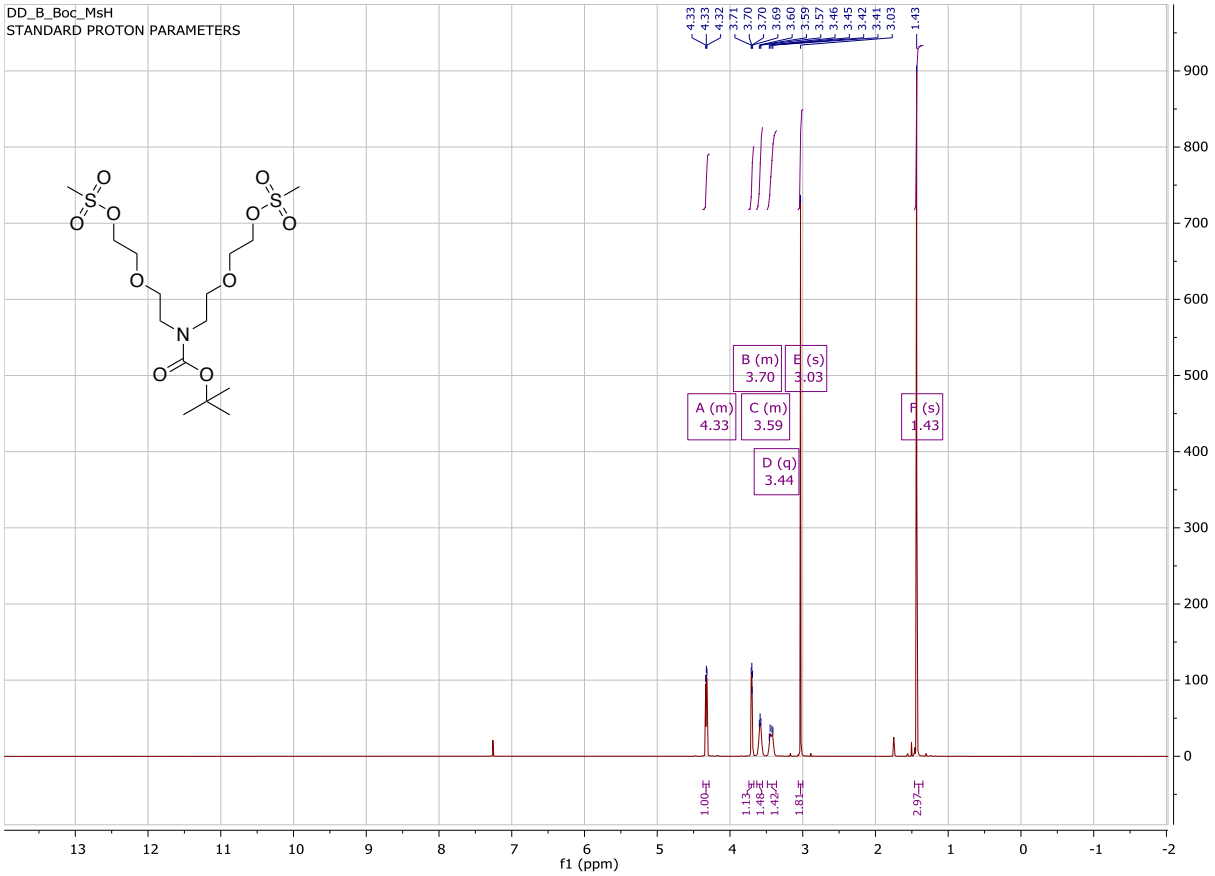

SI.2 - ^{1}H NMR spectra of (**A**) bis-Mesylate and chemical structure. ^{1}H NMR (500 MHz, $CDCl_3$): δ = 4.33 (m, 4H), 3.70 (m, 4H), 3.59 (m, 4H), 3.44 (m, 4H), 3.03 (s, 6H), 1.43 (s, 12H). IR (Film): 2974, 2939, 2874, 1693, 1682, 1545, 1479, 1456, 1416, 1392, 1247, 1172, 1069, 972, 920, 862 cm^{-1}.

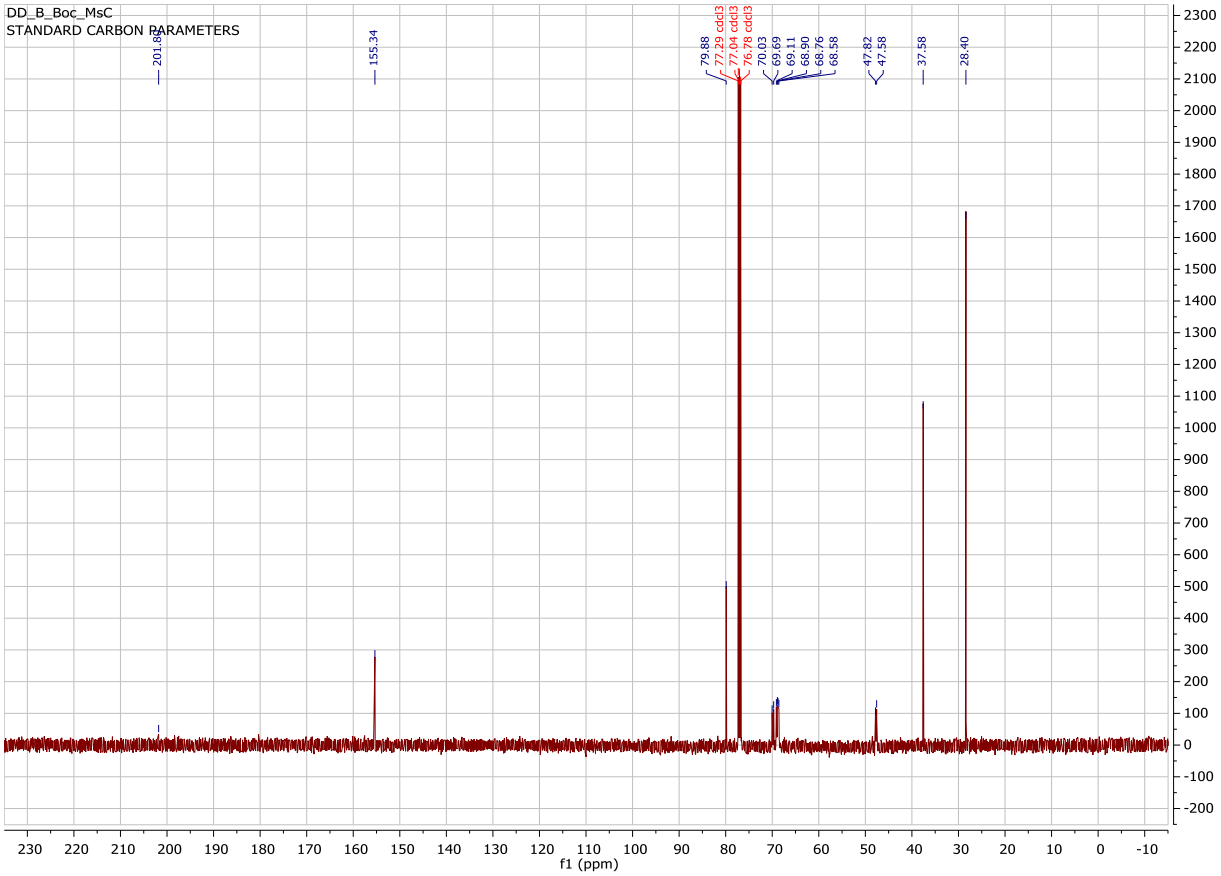

SI.3 - ^{13}C NMR spectra of (**A**) bis-Mesylate. ^{13}C NMR (126 MHz, $CDCl_3$): δ = 155.3, 79.9, 69.9, 68.8, 47.7, 37.6, 28.4. HRMS (EI): m/z calcd for [M+Na] $C_{15}H_{31}NNaO_{10}S_2$ 472.1281. Found 472.1275

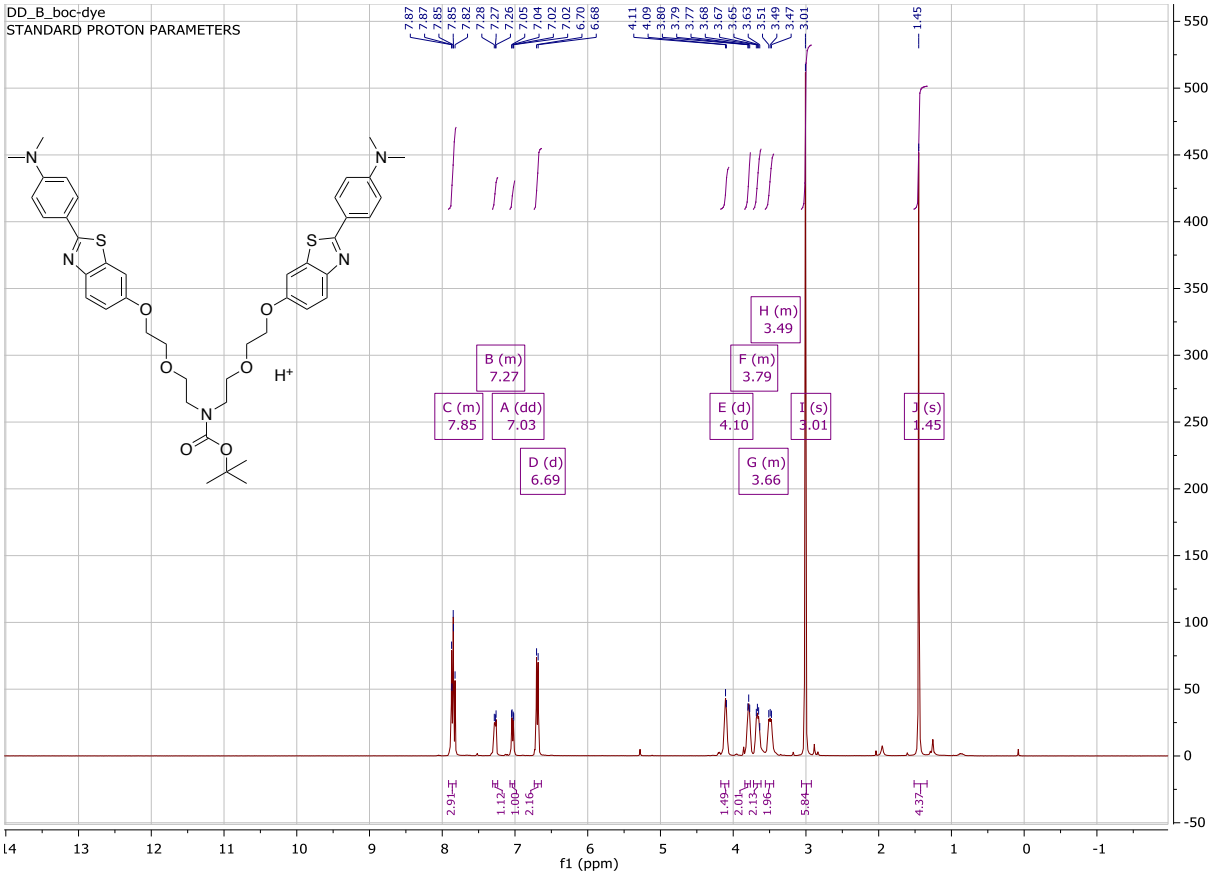

SI.4 - ^{1}H NMR spectra (B) Boc-protected bis-benzothiazole and chemical structure. ^{1}H NMR (500 MHz, $CDCl_3$): δ = 7.91 – 7.81 (m, 6H), 7.31 – 7.24 (m, 2H), 7.03 (dd, *J* = 8.9, 2.5 Hz, 2H), 6.69 (d, *J* = 8.6 Hz, 4H), 4.10 (d, *J* = 4.8 Hz, 2H), 3.84 – 3.76 (m, 4H), 3.72 – 3.62 (m, 4H), 3.56 – 3.44 (m, 4H), 3.01 (s, 12H), 1.45 (s, 9H). IR (Film): 2931, 1684, 1608, 1560, 1410, 1365, 1264, 1226, 1130, 1065, 1006, 967, 943, 864 cm^{-1}.

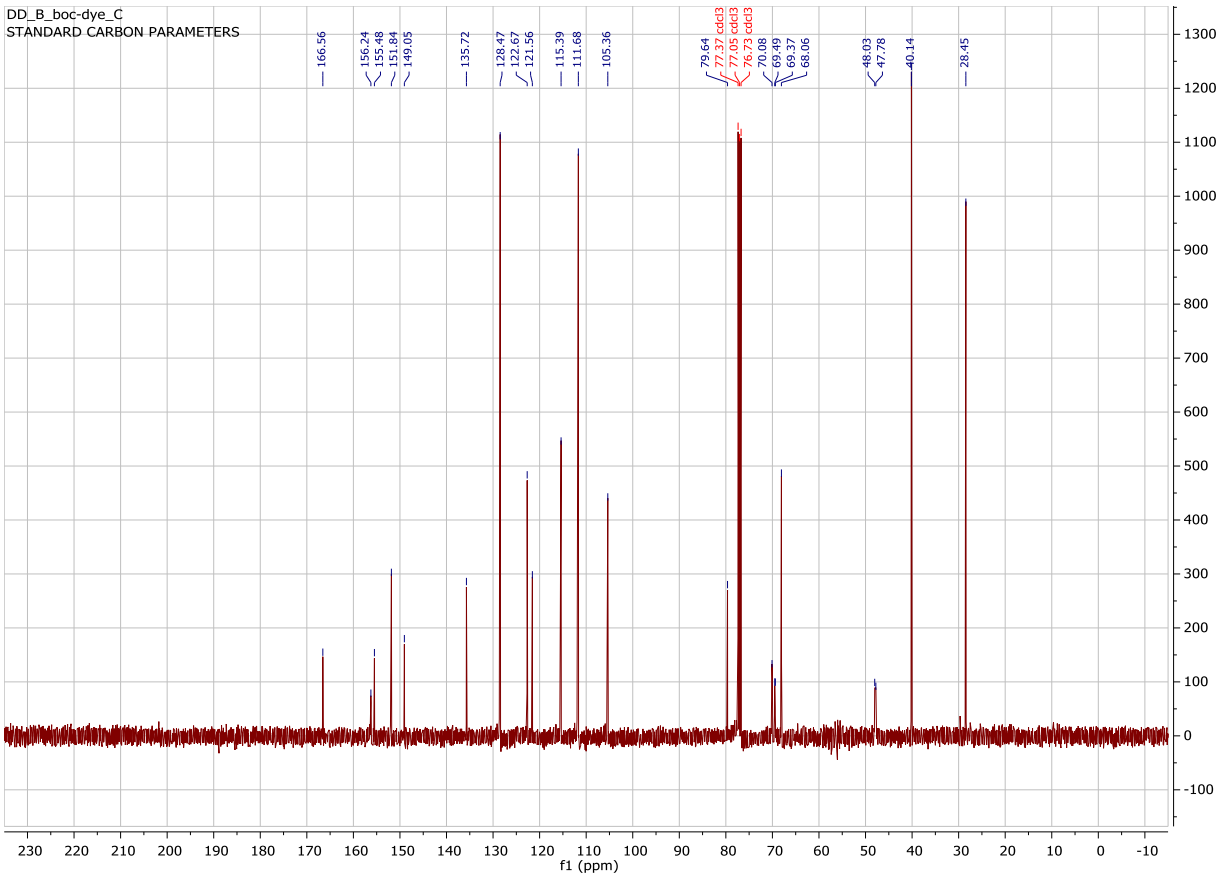

SI.5 – ^{13}C NMR spectra (B) Boc-protected *bis*-benzothiazole. ^{13}C NMR (126 MHz, $CDCl_3$): δ = 166.6, 156.2, 155.5, 151.8, 149.1, 135.7, 128.5, 122.7, 121.6, 115.4, 111.7, 105.4, 79.6, 70.1, 69.5, 69.4, 68.1, 48.0, 47.8, 40.1, 28.5. HRMS (EI): m/z calcd for [M+H] $C_{43}H_{52}N_5O_6S_2$ 798.3359. Found 798.3383.

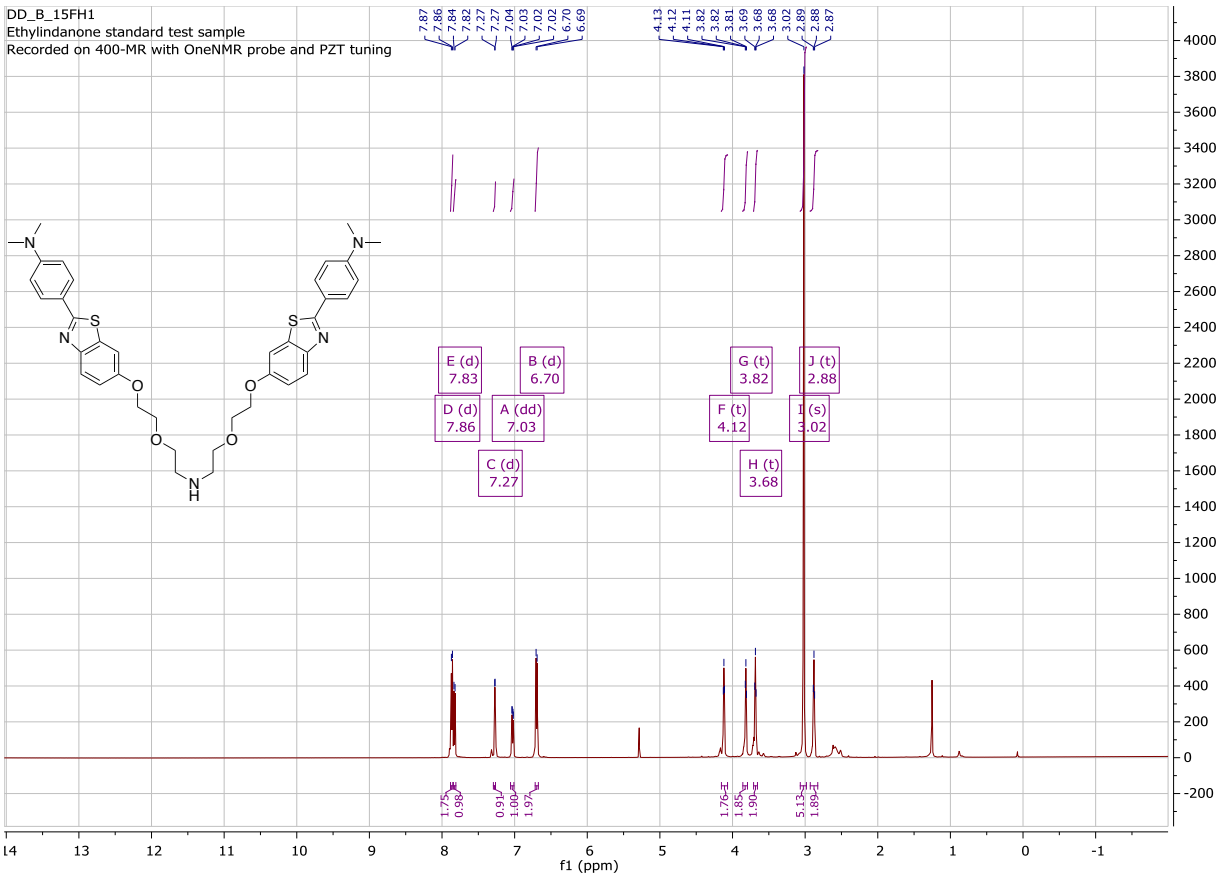

SI.6 - ^{1}H NMR spectra (C) NH *bis*-benzothiazole and chemical structure. ^{1}H NMR (400 MHz, $CDCl_3$): 7.86 (d, J = 8.6 Hz, 4H), 7.83 (d, J = 8.9 Hz, 2H), 7.27 (d, J = 2.5 Hz, 2H), 7.03 (dd, J = 8.9, 2.5 Hz, 2H), 6.70 (d, J = 8.6 Hz, 4H), 4.12 (t, J = 4.7 Hz, 4H), 3.82 (t, J = 4.7 Hz, 4H), 3.68 (t, J = 5.2 Hz, 4H), 3.02 (s, 12H), 2.88 (t, J = 5.2 Hz, 4H). IR (Film): 3401, 2917, 1608, 1560, 1531, 1285, 1263, 1124, 1006, 967, 941, 818 cm^{-1}.

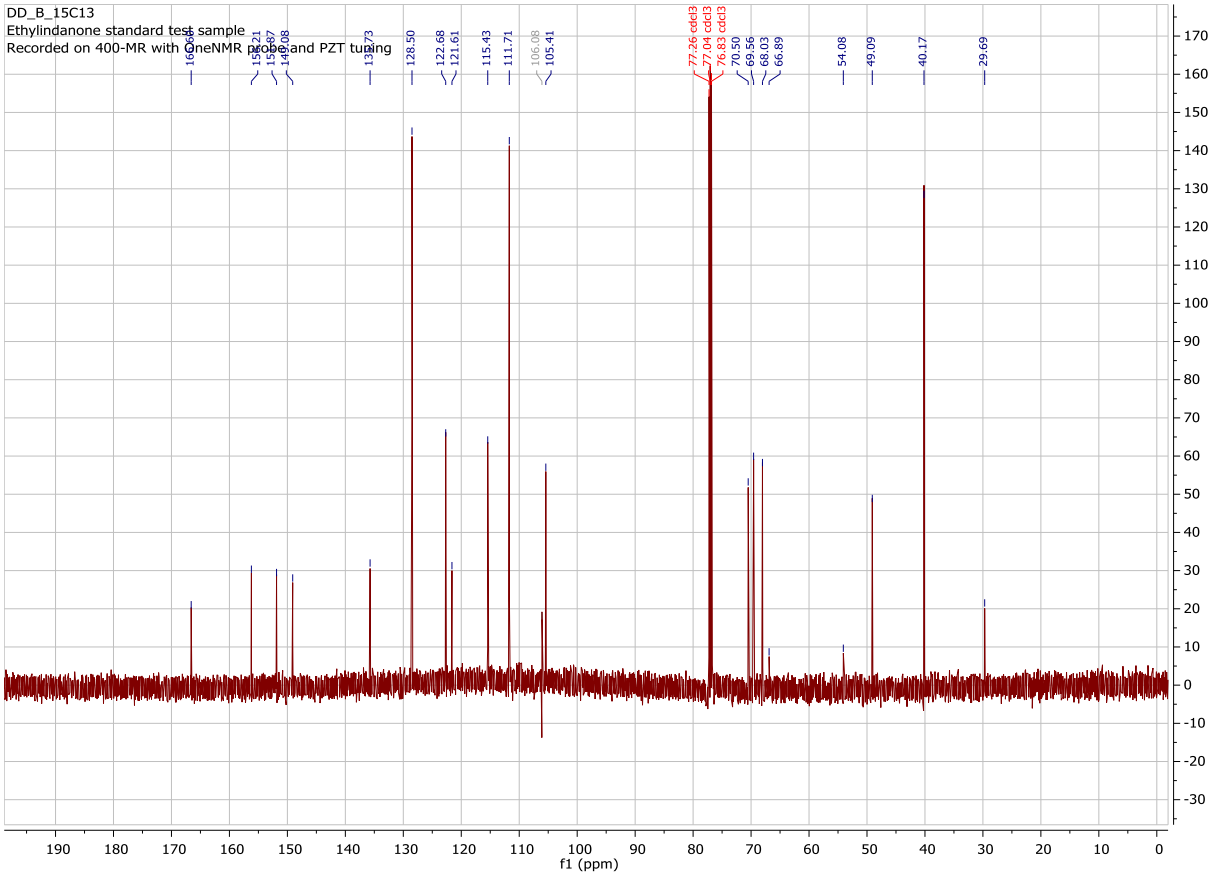

SI.7 – ^{13}C NMR spectra (C) NH *bis*-benzothiazole. Values obtained ^{13}C NMR (126 MHz, $CDCl_3$): δ = 166.6, 156.2, 151.9, 149.1, 135.8, 128.5, 122.7, 121.6, 115.4, 111.7, 106.1, 106.1, 105.4, 70.5, 69.6, 68.0, 49.1, 40.2, 29.7. HRMS (EI): m/z calcd for [M+H] $C_{38}H_{44}N_5O_4S_2$ 698.2835. Found 698.2852.

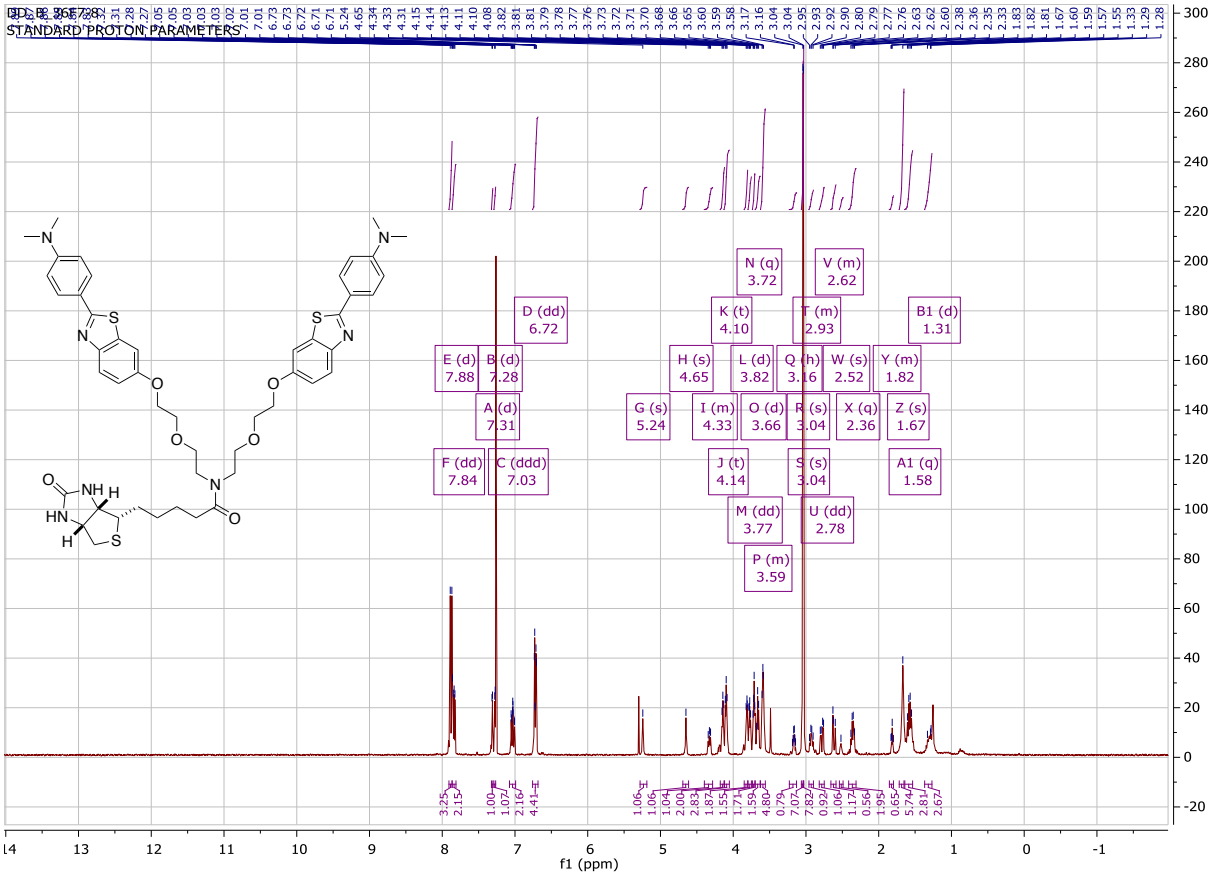

SI.8 - ^{1}H NMR spectra (D) N-Biotinylated *bis*-benzothiazole (**CAP-1**) and chemical structure. ^{1}H NMR (400 MHz, $CDCl_3$): δ = 7.88 (d, *J* = 8.9 Hz, 4H), 7.85 (d, *J* = 8.9, 2H), 7.84 (d, *J* = 8.9, 2H), 7.31 (d, *J* = 2.5 Hz, 1H), 7.28 (d, *J* = 2.5 Hz, 1H), 7.04 (dd, *J* = 8.9, 2.5 Hz, 1H), 7.03 (dd, *J* = 8.9, 2.5 Hz, 1H), 6.73 (d, *J* = 8.9 Hz, 2H), 6.72 (d, *J* = 8.9 Hz, 2H), 5.24 (s, 1H), 4.65 (s, 1H), 4.40 – 4.28 (m, 1H), 4.14 (t, *J* = 4.6 Hz, 2H), 4.10 (t, *J* = 4.6 Hz, 3H), 3.82 (d, *J* = 4.6 Hz, 2H), 3.77 (dd, *J* = 5.5, 3.7 Hz, 2H), 3.72 (q, *J* = 3.1 Hz, 2H), 3.66 (d, *J* = 5.2 Hz, 2H), 3.62 – 3.56 (m, 5H), 3.16 (h, *J* = 3.5 Hz, 1H), 3.05 (s, 6H), 3.04 (s, 6H), 2.96 – 2.90 (m, 1H), 2.78 (dd, *J* = 12.8, 5.0 Hz, 1H), 2.66 – 2.59 (m, 1H), 2.52 (m, 1H), 2.36 (q, *J* = 7.1 Hz, 2H), 1.85 – 1.80 (m, 1H), 1.67 (m, 6H), 1.58 (q, J = 7.5 Hz, 3H), 1.31 (d, J = 16.4 Hz, 3H). IR (Film): 3258, 2929, 1699, 1606, 1560, 1533, 1491, 1366, 1264, 1211, 1126, 1067, 941, 820 cm-1.

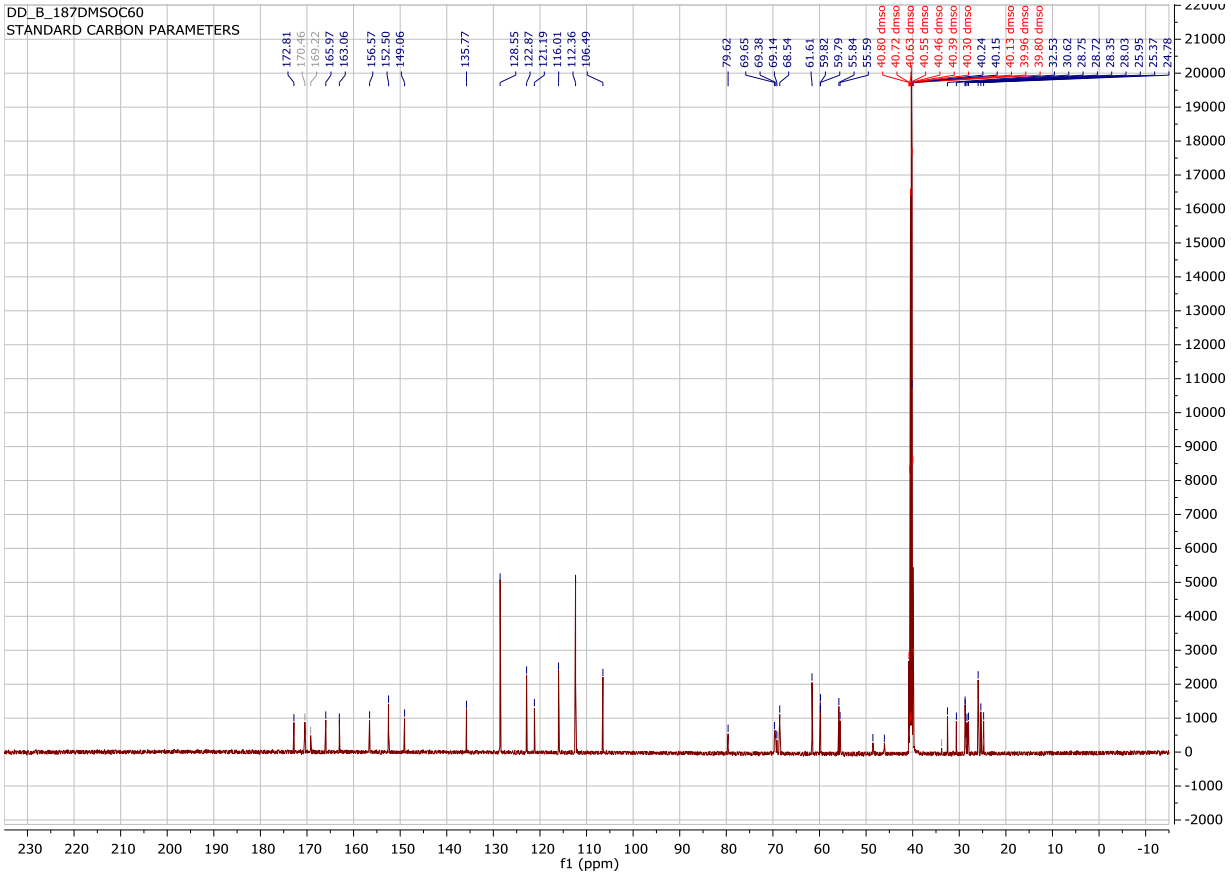

SI.9 - ^{13}C NMR spectra (D) N-Biotinylated *bis*-benzothiazole. ^{13}C NMR (126 MHz, $CDCl_3$) δ = 172.8, 170.5, 169.2, 166.0, 163.1, 156.6, 152.5, 149.1, 135.8, 128.6, 122.9, 121.2, 116.0, 112.4, 106.5, 79.6, 69.7, 69.4, 69.2, 68.6, 61.66, 59.8, 59.8, 55.9, 55.6, 48.6, 46.1, 40.2, 40.2, 32.5, 30.6, 28.8, 28.7, 28.6, 28.4, 28.0, 26.0, 25.7, 25.4, 24.8. HRMS (EI): m/z calcd for [M+H] $C_{48}H_{58}N_7O_6S_3$ 924.3611. Found 924.3618.

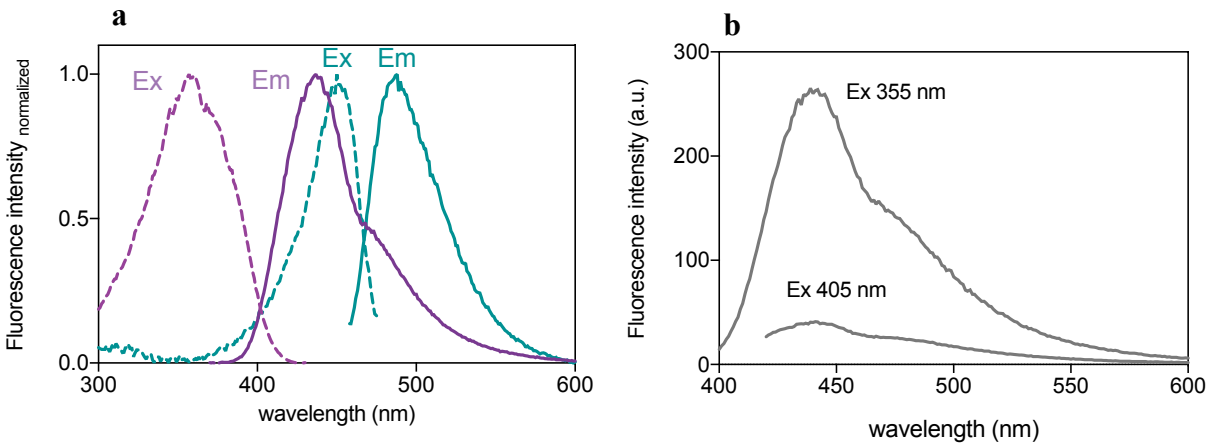

SI.10 – Comparison of spectral properties between CAP-1 and ThT. **a**) Normalized excitation and emission spectrum of 20 μM CAP-1(-) and 20 μM ThT (-) in the presence of 10 μM α-synuclein fibrils. **b**) Decrease in the fluorescence intensity of CAP−1 from using λ_{ex}=355 nm to λ_{ex}=405 nm.

]

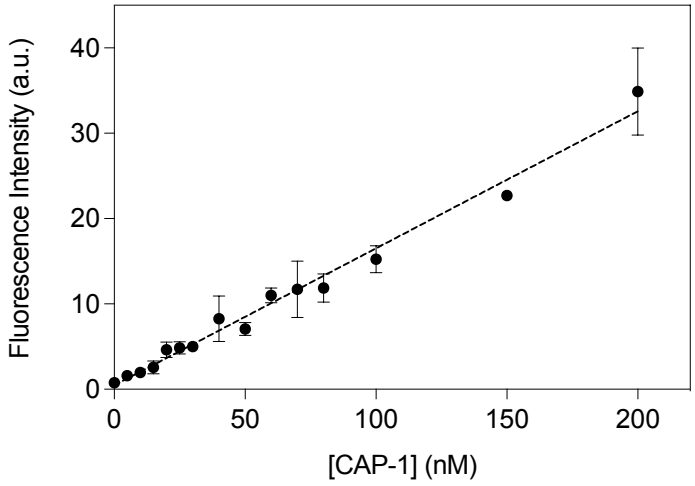

SI.11 – Solubility of CAP-1 in PBS. Maximum fluorescence intensity for each different dilution of CAP-1. Data are presented as the mean ± s.d. of *n = 2* independent experiments and experimental points were fit to a linear regression (R^2=0.9843).

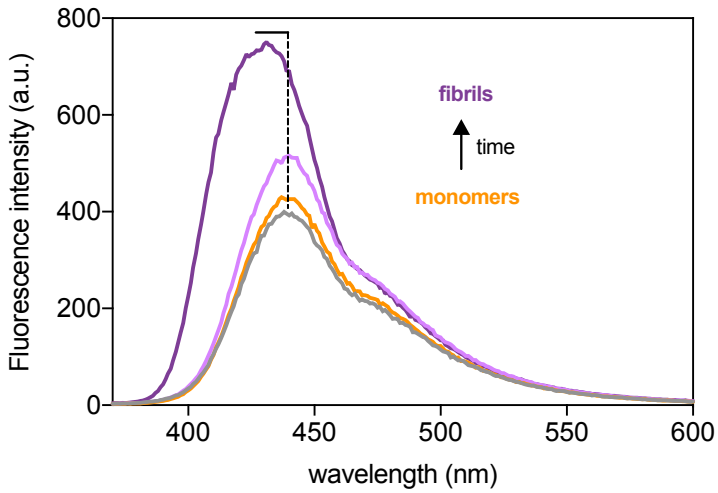

SI.12 - Emission spectra of 20 µM CAP-1 alone and in the presence of different time points of 10 µM α-synuclein aggregation reaction: CAP-1 only (–), t=0h (**– monomers**), t=8h (**– oligomers**) and t=24h (**– fibrils**).

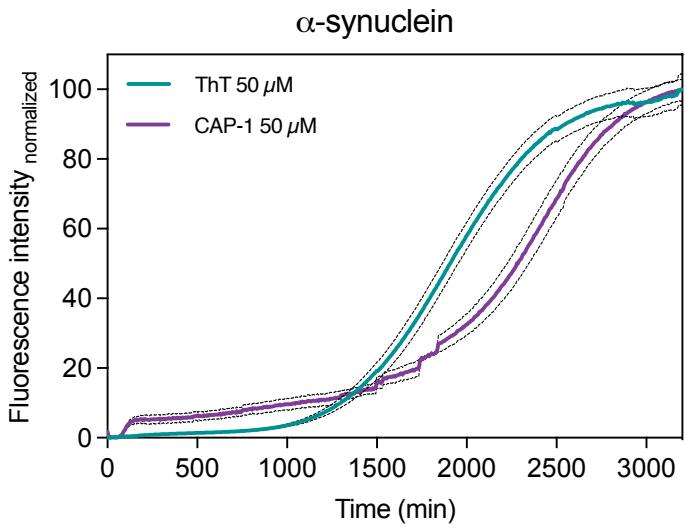

SI. 13 - Normalised aggregation kinetics of α-synuclein in the presence of CAP-1 or ThT. Plate reader assay using 40 μM α-synuclein in the presence of 50 μM CAP-1 (—) or 50 μM ThT (—). The horizontal dashed line (----) represents the SEM of the maximum fluorescence intensity between triplicates from a representative experiment.

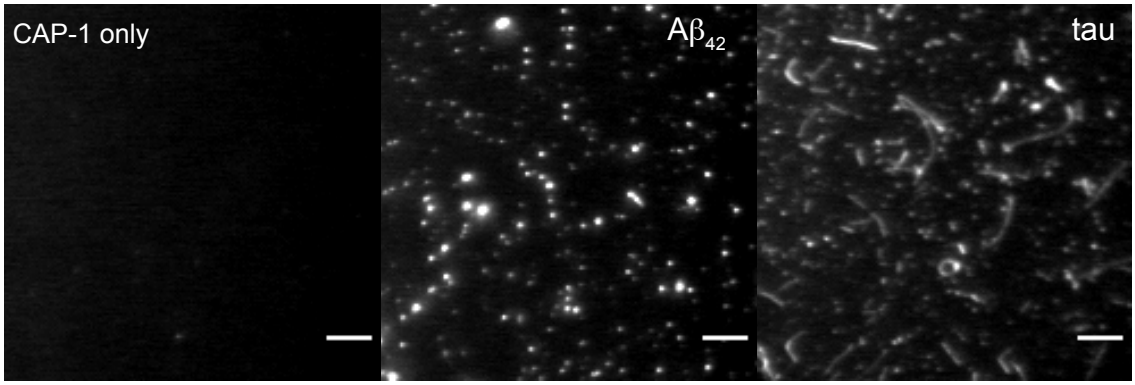

SI.14 - TIRFM images of 5 μM CAP-1 only (left panel), with 1 μM $A\beta_{42}$ (middle) and with 100 nM tau (right). Scale bar = 5 μm. Representative field of view from two independent experiments each with n=16 fields of view.

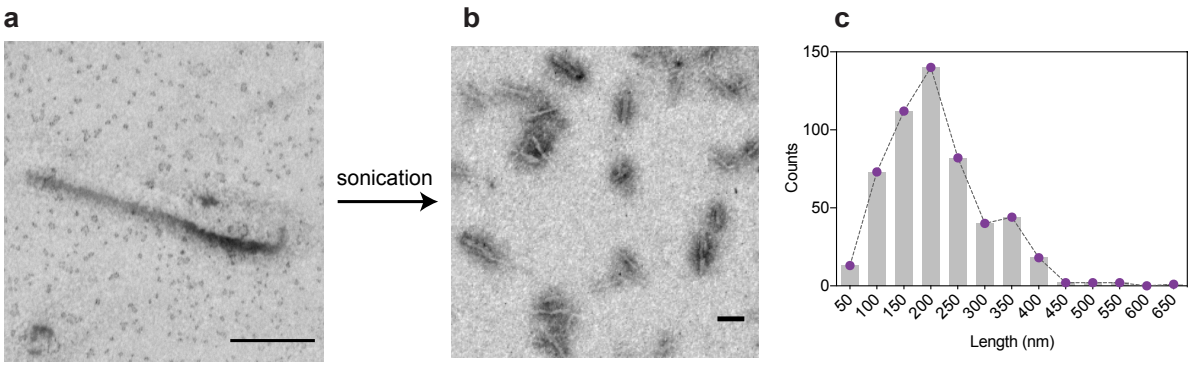

SI.15 - STEM images of α-synuclein fibril before and after sonication probe sonicator. (**a**) fibril length ~3 μm. Scale bar = 1 μm. (**b**) α-synuclein fibrils sonicated, scale bar = 200 nm and (**c**) histogram of fibril length distribution from 549 individual aggregates.

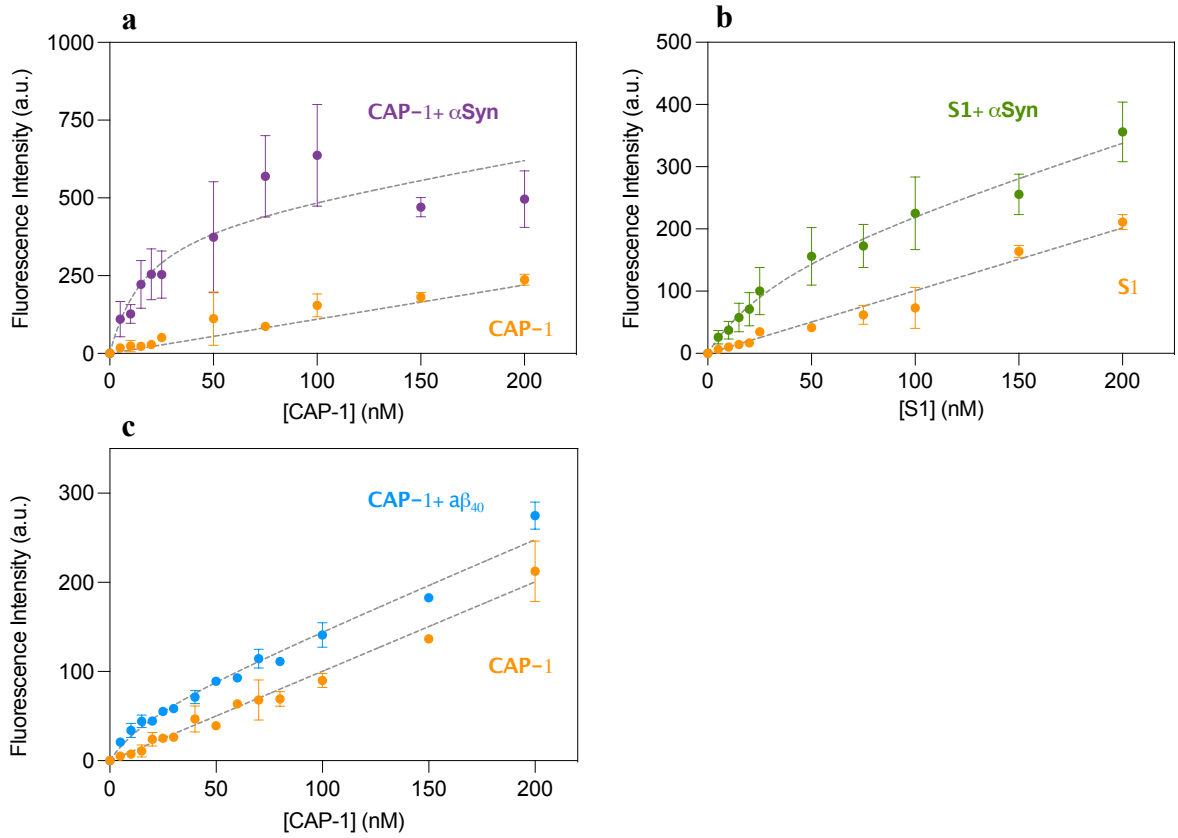

SI.16 - Binding affinity of CAP-1 to α-synuclein or Aβ$_{40}$, and S1 to α-synuclein. Increasing amounts of dye (CAP-1 or S1) were added to 100 nM of α-synuclein or Aβ$_{40}$ fibrils sonicated. At higher concentrations (> 50 nM) the signal in the dye+protein curve is dominated by unbound molecules, so the plot becomes parallel to the dye only curves (**b**) and **c**)). Data are presented as the mean ± s.d. of *n = 3* independent experiments for CAP-1+α-synuclein and S1+α-synuclein and *n = 2* independent experiments for CAP-1 Aβ$_{40}$. The K$_d$ was obtained by fitting the experimental points to a model derived for fluorescent ligands[1–3] , **a**) K$_d$ (CAP-1) = 14.5 ± 5.4 nM, **b**) K$_d$ (S1) = 35 nM ± 12 nM and **c**) K$_d$ (CAP-1) = 17 ± 8 nM. (see Supplementary Information Methods section for more details on data analysis).

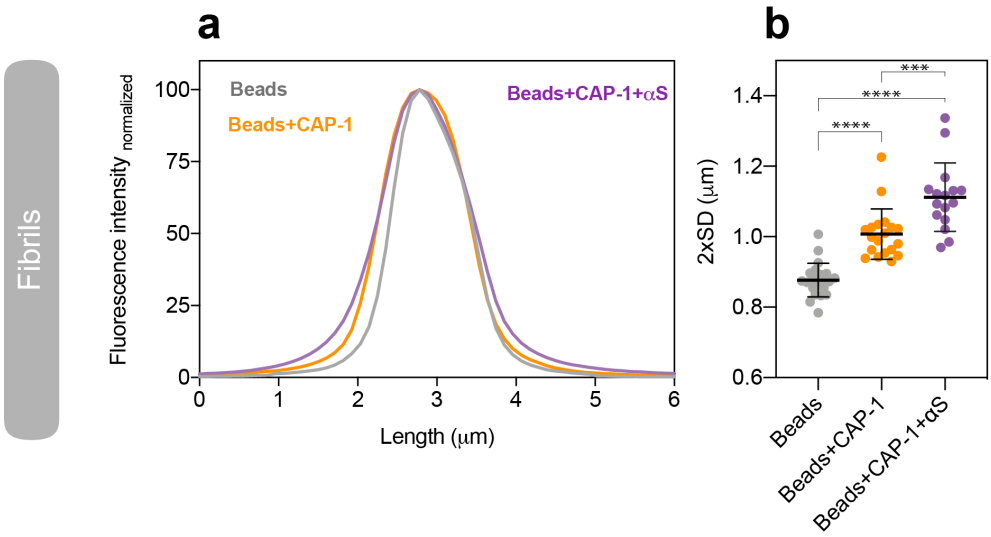

SI.17 - Normalized fluorescence intensity profile of beads. **(a)** Average of intensity profiles for beads alone (—), in the presence of CAP-1 (—) and in the presence of CAP-1 and α-synuclein (—). **(b)** Width of the fluorescence intensity profile measured as the double of the standard deviation (SD) of the Gaussian fitting of the mean of all beads' profiles per sample. Data are presented as the mean ± s.d. of $n > 30$ beads from two independent experiments. One-way ANOVA ($p<0.0001$), and Tukey's post hoc comparisons (**** $p<0.0001$, *** $p=0.0002$).

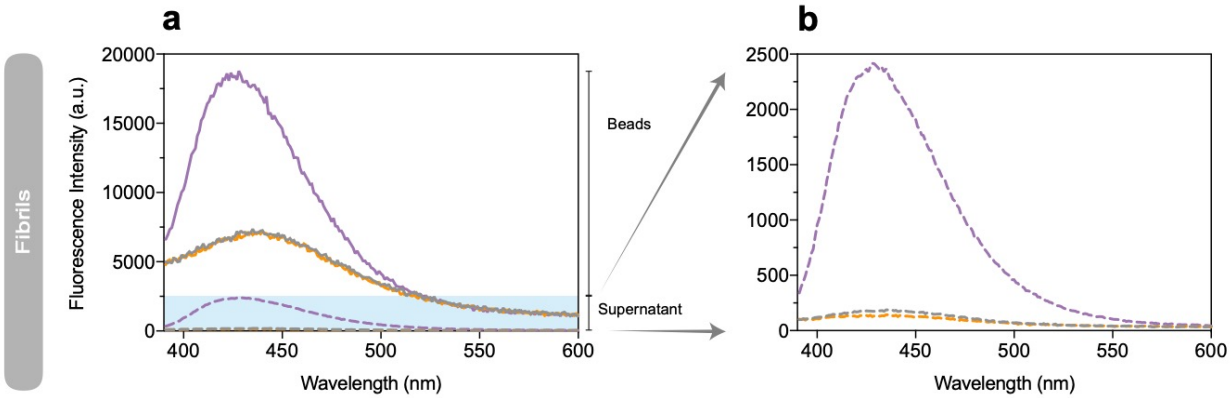

SI.18 - Read-out of protein capture mediated by CAP-1. Emission spectrum of beads and supernatant after AP using 10 μM α-synuclein sonicated fibrils, (**a**) beads (solid line) and supernatant (dashed line) curves together and (**b**) supernatant curves only. Beads+α-synuclein **fibrils** (—), beads+α-synuclein **monomers** (—), beads **only** (—), supernatant+α-synuclein **fibrils** (---), supernatant +α-synuclein **monomers** (---), supernatant **only** (---).

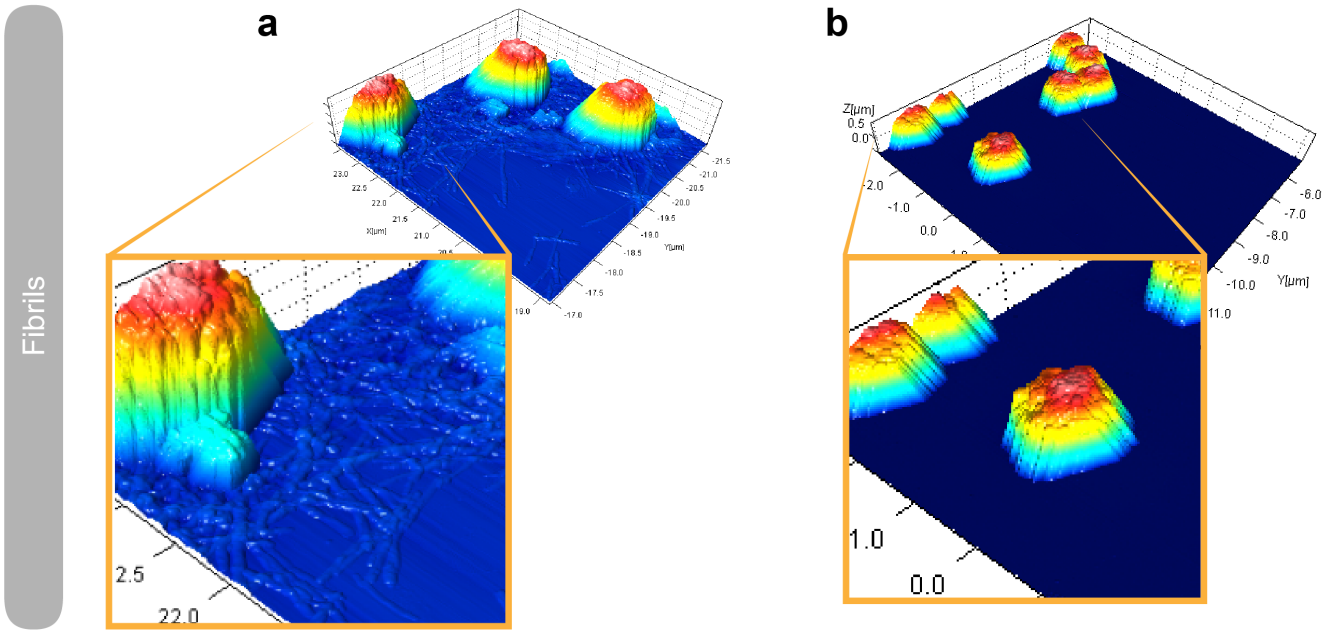

SI.19 - AFM height images after AP in the presence a) and absence b) of α-synuclein fibrils. Fibrils preferentially localize around the beads a).

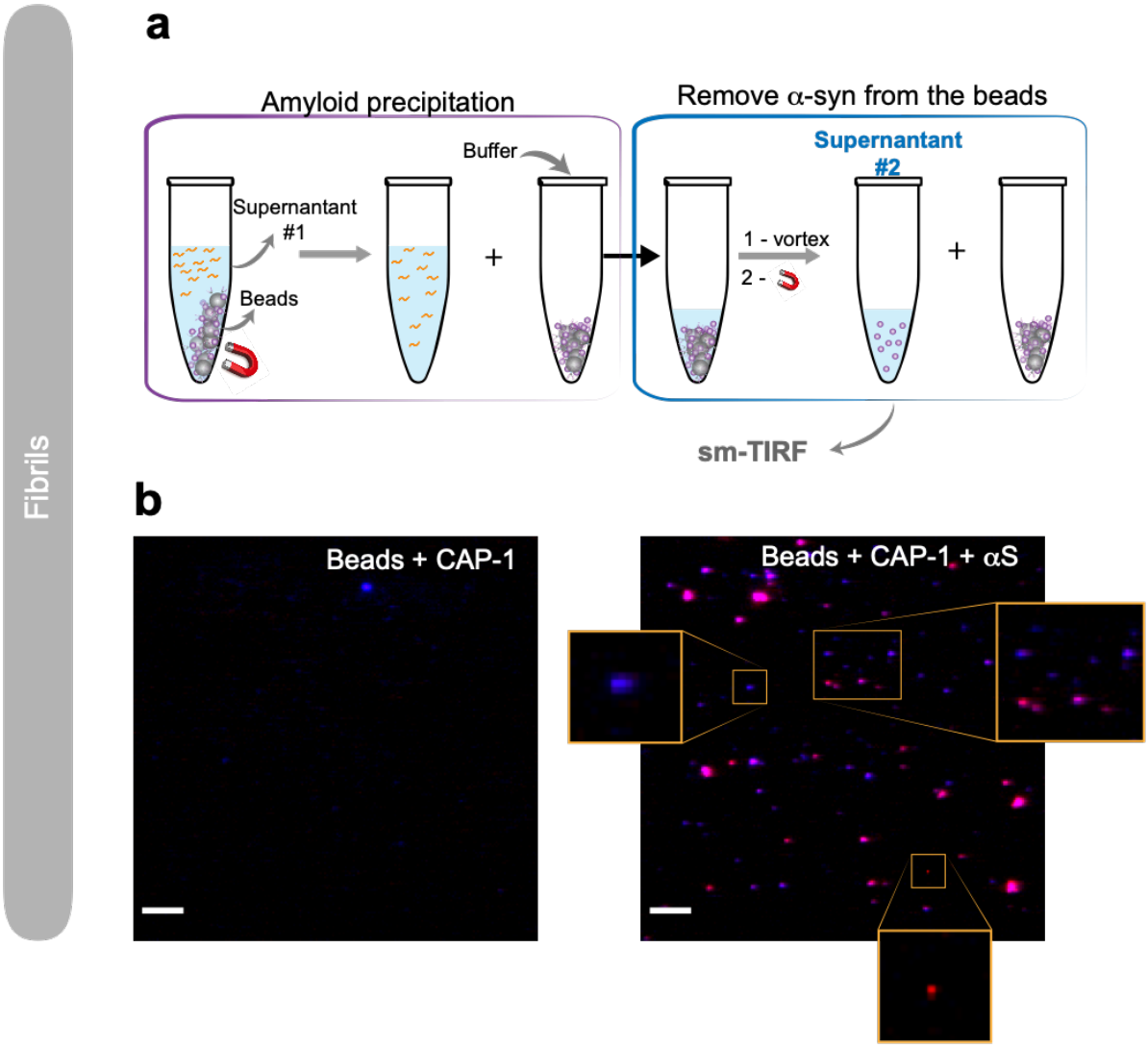

SI.20 - Removal of α-synuclein aggregates from beads. **(a)** Outline of the AP protocol followed by a second dilution and incubation of beads with a small volume of buffer and 5 cycles of 30 sec vortex. **(b)** TIRFM of the new supernatant fraction (#2) after addition of 5 μM ThT. Left, beads+CAP-1 (control) and right beads+CAP-1+ α-synuclein. Images are the result of co-localizing CAP-1 (434/17-25 emission filter - red) and ThT (480/40-25 nm emission filter - blue) channels. The presence of aggregates labelled in blue, red or pink is consistent with the successful removal of aggregates from the beads. Given the reduced overlap between the two channels it is possible to conclude that: aggregates labelled in blue were only labelled by ThT (added prior to imaging) and are therefore free of CAP-1; aggregates labelled in red are aggregates that only have CAP-1 from the beads attached to them; and finally the pink aggregates are larger aggregates where despite the presence of CAP-1 from the beads also ThT found available binding sites. Each image corresponds to a representative field of view from two independent experiments each with *n=16* fields of view.

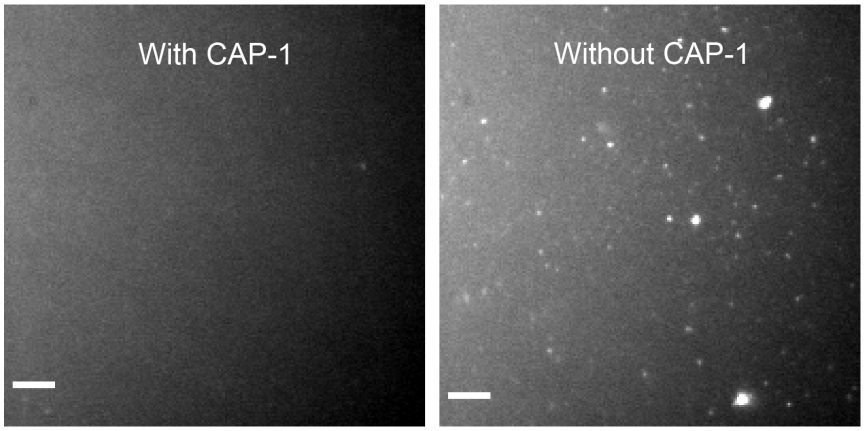

SI.21 - Amyloid-precipitation (AP) of early aggregates. TIRFM images of α-synuclein (t8h) supernatant after AP in the presence (left) and absence (right) of CAP-1. For quantitative comparison on the total number of aggregates removed in the presence of CAP-1 see main text Fig. 2e. Scale bar = 5 μm. Each image corresponds to a representative field of view from *n=27* of one representative experiments.

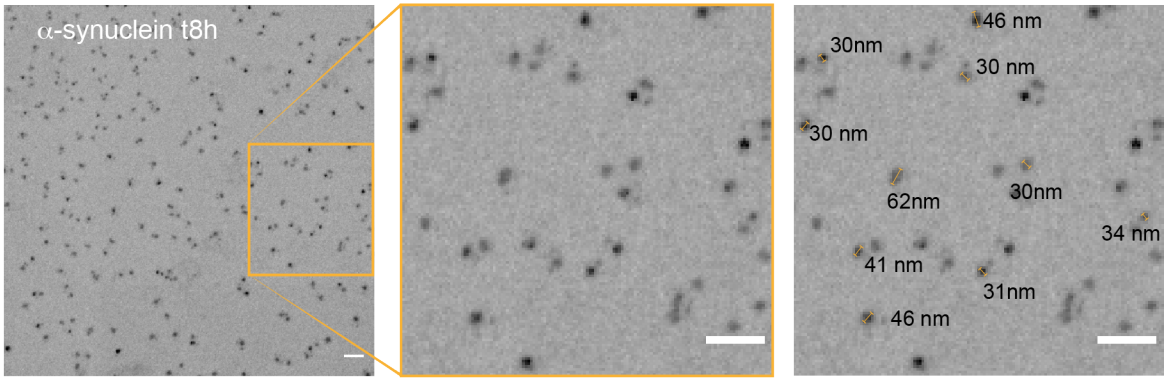

SI.22 - STEM image of α-synuclein oligomers. Left panel, α-synuclein aggregates from t=8h in the aggregation reaction. Middle panel, zoom of area highlighted and right panel size of individual aggregates. Scale bar = 200 nm. Representative field of view from two independent experiments each with *n=4* fields of view.

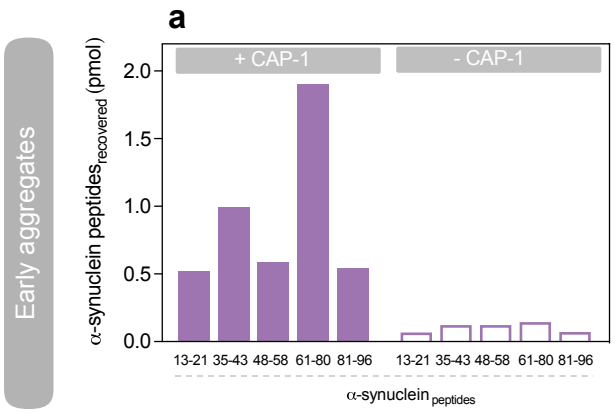

b

Peptide ID	Peptide sequence
α-syn13_21	EGVVAAAEK
α-syn35_43	EGVLYVGSK
α-syn46_58	EGVVHGVATVAEK
α-syn61_80	EQVTNVGGAVVTGVTAVAQK
α-syn81_96	TVEGAGSIAAATGFVK

SI.23 - (a) PRM-MS quantification of α-synuclein peptides recovered after amyloid-precipitation (AP) in presence and absence of CAP-1 using recombinant α-synuclein. **(b)** Table with the amino acid sequence of α-synuclein triptic petides used in the experiment.

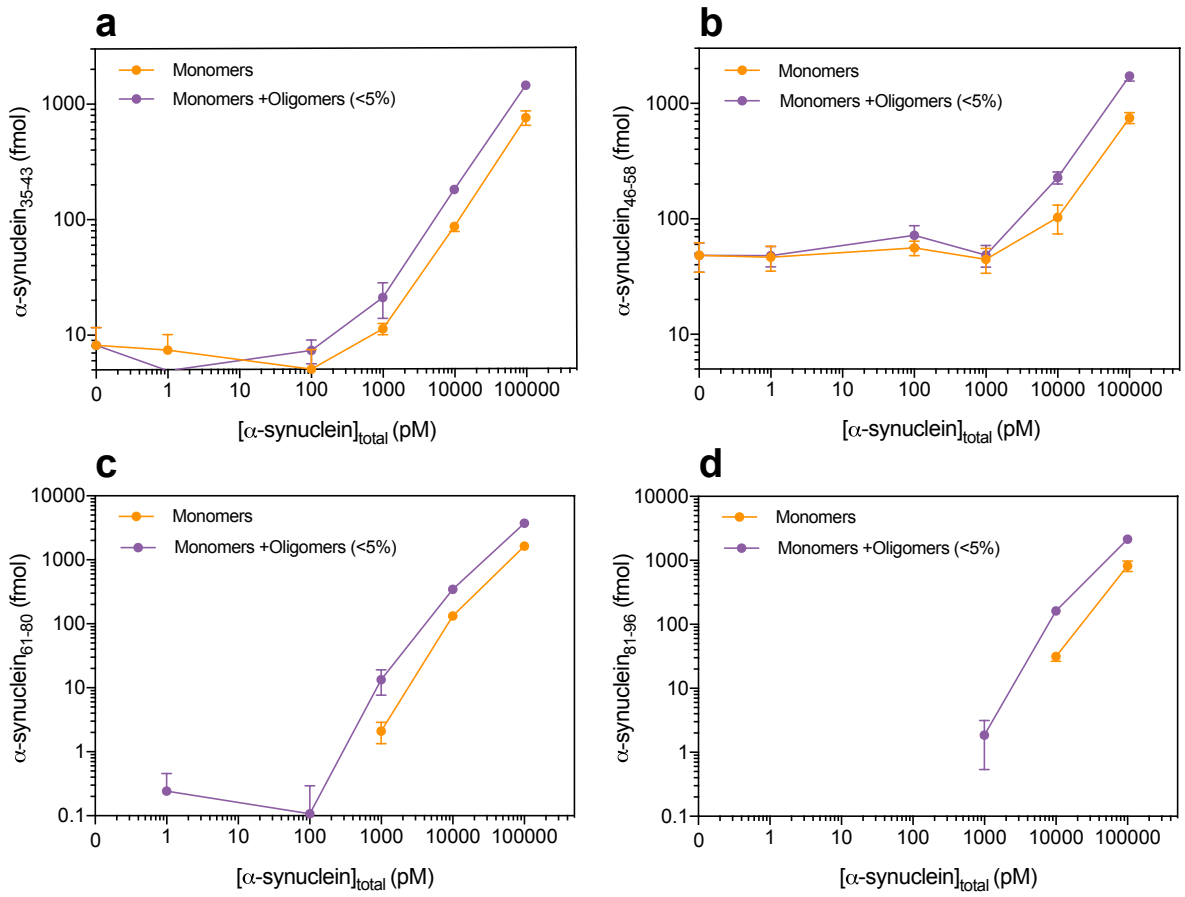

SI.24 - PRM-MS quantification of α-synuclein peptides recovered after amyloid-precipitation (AP) from the background of CSF (complement to Figure 3 of the main text). Prior to AP recombinant α-synuclein (1 pM to 100 nM) monomers or monomers+oligomers were added to control CSF. After AP and on bead digestion the recovered peptides were quantified using PRM-MS **(a)** α-synuclein$_{35\text{-}43}$, **(b)** α-synuclein$_{46\text{-}58}$, **(c)** α-synuclein$_{61\text{-}80}$, **(d)** α-synuclein$_{81\text{-}96}$. Data are presented as the mean ± s.d. of $n = 3$ independent experiments.

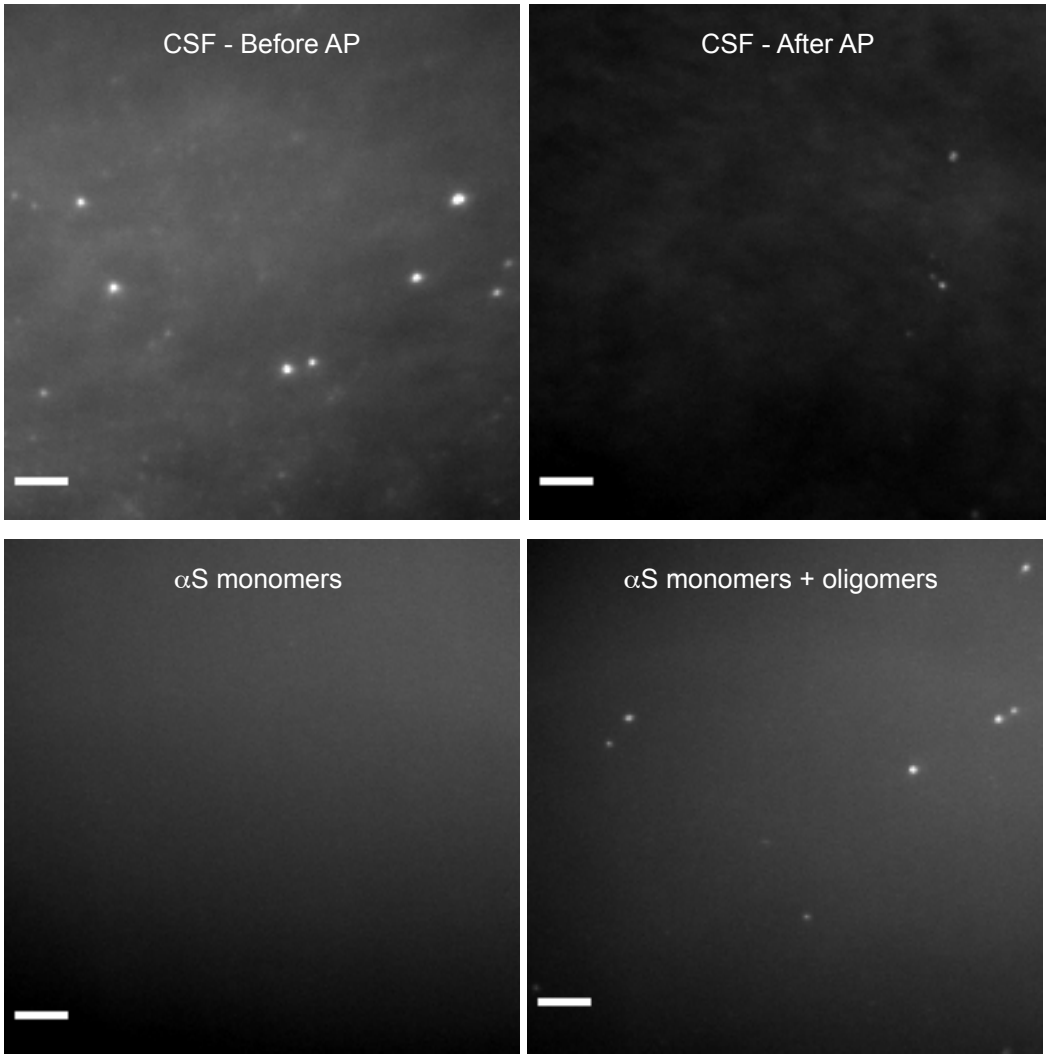

SI.25 - TIRFM images of control CSF and α-synuclein used in Fig. 3b-d. CSF before and after amyloid - precipitation (top panels, left to right), and α-synuclein monomers and monomers+oligomers (bottom panels, left to right). Scale bar = 5 μm. Each image corresponds to a representative field of view from two independent experiments each with *n=27* fields of view

Table 1 - Comparison between **control CSF** proteins pulldown in the presence (+) and absence (-) of CAP-1. Total number of unique proteins present in all replicates and both conditions (presence and absence of CAP-1), exclusive proteins in the presence of CAP-1 and exclusive proteins in the absence of CAP-1 (see Methods for filtering conditions). % of α-helix and % of β-strand determined by protein sequence analysis using PASTA 2.0[4]. Results are from one CSF sample tested in triplicate in each condition (presence and absence of CAP-1). Mean and standard deviation (SD) for the % of α-helix or β-strand predicted for each protein in the different lists (see Table 3-5).

Control CSF	Nr. of proteins	% α-helix	% β-strand
		Mean ± SD	Mean ± SD
Common proteins	44	30 ± 22	20 ± 12
Exclusive (+) CAP-1	21	21 ± 18	25 ± 11
Exclusive (-) CAP-1	4	35 ± 17	19 ± 9

Table 2 - Comparison between **PD CSF** proteins pulldown in the presence (+) and absence (-) of CAP-1. Total number of unique proteins present in all replicates and both conditions (presence and absence of CAP-1), exclusive proteins in the presence of CAP-1 and exclusive proteins in the absence of CAP-1 (see Methods for filtering conditions). % of α-helix and % of β-strand determined by protein sequence analysis using PASTA 2.0[4]. Results are from three different CSF samples tested in triplicate in each condition (presence and absence of CAP-1). Mean and standard deviation (SD) for the % of α-helix or β-strand predicted for each protein in the different lists (see Table 6-8).

PD CSF	Nr. of proteins	% α-helix	% β-strand
		Mean ± SD	Mean ± SD
Common proteins	31	33 ± 24	19 ± 11
Exclusive (+) CAP-1	35	14 ± 14	26 ± 12
Exclusive (-) CAP-1	12	35 ± 31	19 ± 16

Table 3 - List of common proteins pulldown from **control CSF** in the presence and absence of CAP-1 and protein sequence analysis using PASTA 2.0[4]. Results are from one CSF sample tested in triplicate in each condition (presence and absence of CAP-1).

Protein name	length	# amyloids	best energy	% disorder	% α-helix	% β-strand	% coil	UniProtKB accession numbers
Adipocyte enhancer-binding protein 1	1158	20	-6.837548	33.59	22.54	13.47	63.99	Q8IUX7
Amyloid-beta precursor protein	770	20	-20.171292	14.67	46.36	10.78	42.86	P05067
Apolipoprotein D	189	20	-11.361203	4.761	20.63	33.86	45.5	P05090
ıt membrane-specific heparan sulfate proteoglycan core protein	4391	20	-11.599164	1.753	4.12	38.21	57.66	P98160
Collagen alpha-2(I) chain	1366	20	-6.783046	82.86	4.03	8.35	87.63	P08123
Complement C3	1663	20	-15.550313	0.901	24.05	31.03	44.92	P01024
C-X-C motif chemokine 10	98	20	-10.055459	28.57	50	10.2	39.8	P02778
Extracellular matrix protein 2	699	20	-13.318841	27.32	30.19	14.02	55.79	O94769
Fibrinogen alpha chain	866	20	-10.907301	35.33	16.17	24.02	59.82	P02671
Fibronectin	2477	20	-8.093383	4.602	1.7	43.4	54.91	P02751
Fibulin-1	703	20	-14.691325	1.28	12.94	32.29	54.77	P23142
Fibulin-2	1184	20	-7.635911	22.38	11.99	26.52	61.49	P98095
Gelsolin	782	20	-8.072905	12.4	21.74	27.24	51.02	P06396
Growth arrest-specific protein 6	678	20	-7.025432	5.014	22.42	28.76	48.82	Q14393
Hemoglobin subunit beta	147	20	-7.976094	13.6	73.47	0	26.53	P68871
Immunoglobulin kappa constant	107	13	-6.871533	57	1.87	43.93	54.21	P01834
Pleiotrophin	168	20	-8.628732	35.71	45.24	12.5	42.26	P21246
Proteoglycan 4	1404	20	-12.394352	67.8	4.77	15.95	79.27	Q92954
Secretogranin-1	677	3	-5.28399	69.27	39.44	1.92	58.64	P05060
Albumin	609	20	-9.230629	1.97	78	0	22	P02768
Signal peptide, CUB and EGF-like domain-containing protein 1	988	20	-8.710191	5.263	10.02	31.07	58.91	Q8IWY4
SPARC-like protein 1	664	0	-4.875821	64.9	30.57	9.64	59.79	Q14515
Spondin-1	807	20	-7.521185	8.55	26.89	16.6	56.51	Q9HCB6
Transthyretin	147	20	-8.269028	12.92	21.09	29.93	48.98	P02766
Vitamin K-dependent protein S	676	20	-7.754854	3.106	21.45	29.14	49.41	P07225
Actin, cytoplasmic 1	375	5	-6.030025	1.866	34.13	18.4	47.47	P60709
Alpha-2-HS-glycoprotein	367	18	-6.731075	14.16	24.52	23.43	52.04	P02765
Angiotensinogen	485	20	-7.332547	7.422	40	12.99	47.01	P01019
Apolipoprotein A-I	267	20	-7.585395	6.367	91.39	0	8.61	P02647
Apolipoprotein E	317	20	-7.905302	6.94	90.54	0	9.46	P02649
Carboxypeptidase E	476	20	-8.888563	10.5	34.87	17.44	47.69	P16870
Clusterin	449	20	-7.161453	6.458	64.14	5.35	30.51	P10909
EGF-containing fibulin-like extracellular matrix protein 1	493	20	-9.719066	4.665	5.68	36.11	58.21	Q12805
Extracellular superoxide dismutase [Cu-Zn]	240	20	-6.904548	24.16	26.67	22.92	50.42	P08294
Fibrinogen beta chain	491	20	-10.265117	9.979	31.57	21.38	47.05	P02675
Fibrinogen gamma chain	453	20	-10.663145	9.05	29.58	25.17	45.25	P02679
Glyceraldehyde-3-phosphate dehydrogenase	335	20	-6.530456	2.686	26.27	27.16	46.57	P04406
Immunoglobulin heavy constant gamma 1	330	20	-8.945009	13.63	6.36	33.33	60.3	P01857
Monocyte differentiation antigen CD14	375	4	-5.199154	5.866	36	12.27	51.73	P08571
Osteopontin	314	20	-10.253145	95.54	14.33	8.92	76.75	P10451
Phospholipid transfer protein	493	20	-8.704384	5.07	30.43	23.94	45.64	P55058
Prothrombin	622	9	-6.070176	1.929	30.39	14.47	55.14	P00734
Secreted frizzled-related protein 3	325	2	-5.784988	15.69	29.54	13.54	56.92	Q92765
Vitronectin	478	20	-7.916569	29.07	16.53	20.29	63.18	P04004
Mean (%)					**29.7**	**19.8**		
SD					22.0	11.8		

Table 4 - List of exclusive proteins pulldown from **control CSF** in the presence of CAP-1 and protein sequence analysis using PASTA 2.0[4]. Results are from one CSF sample tested in triplicate in each condition (presence and absence of CAP-1).

Protein name	length	# amyloids	best energy	% disorder	% α-helix	% β-strand	% coil	UniProtKB accession numbers
Calsyntenin-1	981	20	-23.180393	11.82	14.58	34.86	50.56	O94985
Ceruloplasmin	1065	20	-9.458505	1.314	7.61	40	52.39	P00450
Coagulation factor V	2224	20	-10.169181	16.18	13.98	24.82	61.2	P12259
Collagen alpha-1(XIV) chain	1796	20	-11.613298	22.77	17.48	27.23	55.29	Q05707
Collagen alpha-1(XVIII) chain	1754	20	-9.187466	62.59	12.31	12.26	75.43	P39060
Complement C1r subcomponent	705	20	-7.21306	2.836	9.79	34.04	56.17	P00736
Complement C1s subcomponent	688	20	-10.45933	1.453	4.36	34.01	61.63	P09871
Complement factor H	1231	20	-10.155511	0.974	2.44	38.51	59.06	P08603
Cystatin-C	146	20	-8.518981	31.5	33.56	15.75	50.68	P01034
Hemoglobin subunit alpha	142	8	-6.722631	9.859	69.01	0	30.99	P69905
Pre-B-cell leukemia transcription factor-interacting protein 1	731	20	-8.736379	63.06	43.37	6.84	49.79	Q96AQ6
Prostaglandin-H2 D-isomerase	190	5	-5.703427	5.789	31.58	23.68	44.74	P41222
Beta-Ala-His dipeptidase	506	20	-8.626567	1.976	42.69	14.82	42.49	Q96KN2
Complement C1q subcomponent subunit B	253	20	-8.602751	37.15	7.91	30.04	62.06	P02746
Complement C1q subcomponent subunit C	245	20	-10.420788	35.91	5.71	30.2	64.08	P02747
Complement component C9	559	20	-8.159938	6.082	23.43	23.97	52.59	P02748
EGF-containing fibulin-like extracellular matrix protein 2	443	20	-7.246752	11.28	9.71	29.57	60.72	O95967
Fibulin-5	448	20	-11.868578	1.339	0	40.18	59.82	Q9UBX5
Heparin cofactor 2	499	20	-9.391957	9.819	40.88	17.23	41.88	P05546
Lactadherin	387	20	-8.356042	1.291	20.67	29.72	49.61	Q08431
Major prion protein	253	20	-16.038002	35.96	32.02	11.46	56.52	P04156
Mean (%)					**21.1**	**24.7**		
SD					17.5	11.3		

Table 5 - List of exclusive proteins pulldown from **control CSF** in the absence of CAP-1 and protein sequence analysis using PASTA 2.0[4]. Results are from one CSF sample tested in triplicate in each condition (presence and absence of CAP-1).

Protein name	length	# amyloids	best energy	% disorder	% α-helix	% β-strand	% coil	UniProtKB accession numbers
Band 3 anion transport protein	911	20	-27.518775	12.29	60.26	6.48	33.26	P02730
Complement C4-A	1744	20	-8.773181	1.777	26.26	27.24	46.5	P0C0L4
Vitamin K-dependent protein C	461	20	-7.204106	7.375	32.1	18.66	49.24	P04070
Coagulation factor X	488	20	-7.08814	9.221	21.72	23.98	54.3	P00742
Mean (%)					**35.1**	**19.1**		
SD					17.3	9.1		

Table 6 - List of common proteins pulldown from **PD CSF** in the presence and absence of CAP-1 and protein sequence analysis using PASTA 2.0[4]. Results are from three different CSF samples tested in triplicate in each condition (presence and absence of CAP-1).

Protein name	length	# amyloids	best energy	% disorder	% α-helix	% β-strand	% coil	UniProtKB accession numbers
Adipocyte enhancer-binding protein 1	1158	20	-6.837548	33.59	22.54	13.47	63.99	Q8IUX7
Angiogenin	147	20	-10.376892	7.482	22.45	25.85	51.7	P03950
Apolipoprotein D	189	20	-11.361203	4.761	20.63	33.86	45.5	P05090
Calsyntenin-1	981	20	-23.180393	11.82	14.58	34.86	50.56	O94985
Fibrinogen alpha chain	866	20	-10.907301	35.33	16.17	24.02	59.82	P02671
Fibronectin	2477	20	-8.093383	4.602	1.7	43.4	54.91	P02751
Inactive carboxypeptidase-like protein X2	756	20	-8.010832	19.84	21.3	22.62	56.08	Q8N436
Latent-transforming growth factor beta-binding protein 2	1821	18	-5.602549	23.66	6.04	24.05	69.91	Q14767
Matrix Gla protein	103	20	-11.076716	10.67	84.47	0	15.53	P08493
Pleiotrophin	168	20	-8.628732	35.71	45.24	12.5	42.26	P21246
Prostaglandin-H2 D-isomerase	190	5	-5.703427	5.789	31.58	23.68	44.74	P41222
Proteoglycan 4	1404	20	-12.394352	67.8	4.77	15.95	79.27	Q92954
Ribonuclease pancreatic	156	20	-15.116791	30.12	25.64	28.85	45.51	P07998
Albumin	609	20	-9.230629	1.97	78	0	22	P02768
Signal peptide, CUB and EGF-like domain-containing protein 1	988	20	-8.710191	5.263	10.02	31.07	58.91	Q8IWY4
Spondin-1	807	20	-7.521185	8.55	26.89	16.6	56.51	Q9HCB6
Transthyretin	147	20	-8.269028	12.92	21.09	29.93	48.98	P02766
Apolipoprotein A-I	267	20	-7.585395	6.367	91.39	0	8.61	P02647
Apolipoprotein E	317	20	-7.905302	6.94	90.54	0	9.46	P02649
Clusterin	449	20	-7.161453	6.458	64.14	5.35	30.51	P10909
Fibrinogen beta chain	491	20	-10.265117	9.979	31.57	21.38	47.05	P02675
Fibrinogen gamma chain	453	20	-10.663145	9.05	29.58	25.17	45.25	P02679
Glia-derived nexin	398	20	-9.936162	1.758	28.14	27.89	43.97	P07093
Glyceraldehyde-3-phosphate dehydrogenase	335	20	-6.530456	2.686	26.27	27.16	46.57	P04406
Major prion protein	253	20	-16.038002	35.96	32.02	11.46	56.52	P04156
Mimecan	298	20	-6.921483	1.677	27.85	18.12	54.03	P20774
Olfactomedin-like protein 3	406	20	-9.374003	2.955	30.05	20.69	49.26	Q9NRN5
Phospholipid transfer protein	493	20	-8.704384	5.07	30.43	23.94	45.64	P55058
Secreted frizzled-related protein 3	325	2	-5.784988	15.69	29.54	13.54	56.92	Q92765
Secreted frizzled-related protein 4	346	20	-10.232728	23.41	44.22	5.2	50.58	Q6FHJ7
SPARC-related modular calcium-binding protein 1	434	20	-7.035247	15.66	24.42	16.36	59.22	Q9H4F8
Mean (%)					**33.3**	**19.3**		
SD					24.0	11.2		

Table 7 - List of exclusive proteins pulldown from **PD CSF** in the presence of CAP-1 and protein sequence analysis using PASTA 2.0[4]. Results are from three different CSF samples tested in triplicate in each condition (presence and absence of CAP-1).

Protein name	length	# amyloids	best energy	% disorder	% α-helix	% β-strand	% coil	UniProtKB accession numbers
nt membrane-specific heparan sulfate proteoglycan core protein	377	20	-8.945009	18.56	5.84	30.77	63.4	P98160
Coagulation factor V	2224	20	-10.169181	16.18	13.98	24.82	61.2	P12259
Collagen alpha-1(I) chain	1464	7	-5.272464	79.37	2.12	8.33	89.55	P02452
Collagen alpha-1(XVIII) chain	1754	20	-9.187466	62.59	12.31	12.26	75.43	P39060
Collagen alpha-2(I) chain	1366	20	-6.783046	82.86	4.03	8.35	87.63	P08123
Complement C4-A	1744	20	-8.773181	1.777	26.26	27.24	46.5	P0C0L4
Complement factor H	1231	20	-10.155511	0.974	2.44	38.51	59.06	P08603
Elastin	786	14	-7.851138	11.83	21.88	1.15	76.97	P15502
Fibrillin-1	2871	20	-7.913752	3.065	4.25	31.8	63.95	P35555
Fibulin-1	703	20	-14.691325	1.28	12.94	32.29	54.77	P23142
Fibulin-2	1184	20	-7.635911	22.38	11.99	26.52	61.49	P98095
Gelsolin	782	20	-8.072905	12.4	21.74	27.24	51.02	P06396
Immunoglobulin kappa light chain	214	13	-6.871533	32.71	4.67	42.52	52.8	P0DOX7
Latent-transforming growth factor beta-binding protein 1	1721	20	-7.848722	14.93	6.16	26.84	67	Q14766
Macrophage receptor MARCO	520	20	-19.116756	59.23	18.46	12.31	69.23	Q9UEW3
Matrilin-2	956	20	-8.212839	9.623	29.18	29.39	41.42	O00339
Papilin	1278	20	-6.706005	32.39	2.97	28.79	68.23	O95428
Probable carboxypeptidase X1	734	11	-5.605048	10.62	19.48	25.07	55.45	Q96SM3
venger receptor cysteine-rich domain-containing protein SSC5D	1573	9	-6.311401	57.21	8.52	14.94	76.54	A1L4H1
Target of Nesh-SH3	1075	20	-11.356688	42.88	4.47	27.07	68.47	Q7Z7G0
Tenascin-X	4244	20	-8.156655	13.03	1.84	38.81	59.35	P22105
C4b-binding protein alpha chain	597	20	-7.953199	5.192	10.72	36.18	53.1	P04003
Chondroadherin	359	20	-7.114148	12.25	57.1	1.95	40.95	O15335
Complement C1q subcomponent subunit C	245	20	-10.420788	35.91	5.71	30.2	64.08	P02747
EGF-containing fibulin-like extracellular matrix protein 1	493	20	-9.719066	4.665	5.68	36.11	58.21	Q12805
EGF-containing fibulin-like extracellular matrix protein 2	443	20	-7.246752	11.28	9.71	29.57	60.72	O95967
Fibulin-5	448	20	-11.868578	1.339	0	40.18	59.82	Q9UBX5
Glutaminyl-peptide cyclotransferase	361	20	-8.459151	2.216	45.43	9.7	44.88	Q16769
Immunoglobulin heavy constant alpha 1	353	20	-8.311744	20.39	12.18	31.73	56.09	P01876
Immunoglobulin heavy constant gamma 3	4390	20	-11.599164	1.753	3.96	38.45	57.59	P01860
Immunoglobulin mu heavy chain	576	20	-13.628103	2.604	1.74	48.26	50	P0DOX6
16270|IBP7_HUMAN Insulin-like growth factor-binding protein 7	282	12	-6.416259	10.63	8.16	28.37	63.48	Q16270
Lysyl oxidase homolog 1	574	20	-8.110721	45.64	10.63	21.6	67.77	Q08397
Prothrombin	622	9	-6.070176	1.929	30.39	14.47	55.14	P00734
Secreted frizzled-related protein 2	295	3	-6.152469	3.728	44.75	12.2	43.05	Q96HF1
Mean (%)					**13.8**	**25.5**		
SD					13.7	11.8		

Table 8 – List of exclusive proteins pulldown from **PD CSF** in the absence of CAP-1 and protein sequence analysis using PASTA 2.0[4]. Results are from three different CSF samples tested in triplicate in each condition (presence and absence of CAP-1).

Protein name	length	# amyloids	best energy	% disorder	% α-helix	% β-strand	% coil	UniProtKB accession numbers
Apolipoprotein A-II	100	20	-7.08197	10	86	0	14	P02652
Apolipoprotein C-III	99	20	-9.551744	21.21	84.85	0	15.15	P02656
Cadherin-1	882	20	-15.327144	15.64	10.09	36.73	53.17	P12830
C-reactive protein	143	16	-6.941046	27.97	20.98	26.57	52.45	P02741
Cystatin-C	146	20	-8.518981	31.5	33.56	15.75	50.68	P01034
Hornerin	2850	20	-9.874367	97.47	2.63	7.44	89.93	Q86YZ3
Midkine	224	20	-6.492262	3.571	3.13	50	46.88	P21741
Protocadherin alpha-9	950	20	-24.095895	26.73	9.05	34.74	56.21	Q9Y5H5
Sodium/iodide cotransporter	643	20	-29.572005	9.02	59.41	4.51	36.08	Q92911
Stromal cell-derived factor 1	93	20	-15.459366	6.451	63.44	11.83	24.73	P48061
Shadow of prion protein	151	0	-4.344823	51.65	27.81	15.89	56.29	Q5BIV9
Sushi repeat-containing protein SRPX	464	20	-7.759716	10.34	20.26	29.96	49.78	P78539
Mean (%)					**35.1**	**19.5**		
SD					30.6	16.1		

Table 9 – Comparison between the total number of proteins and amyloid proteins for both samples, control and PD CSF, in the presence (+) and absence (-) of CAP-1 determined by the web server RFAmyloid[5].

	Total nr. proteins		**Amyloid proteins**	
	(+) CAP-1	(-) CAP-1	(+) CAP-1	(-) CAP-1
Control CSF	65	48	37	27
PD CSF	66	43	38	27

References

1. Stein, R. A., Wilkinson, J. C., Guyer, C. A. & Staros, J. V. An analytical approach to the measurement of equilibrium binding constants: Application to EGF binding to EGF receptors in intact cells measured by flow cytometry. *Biochemistry* **40**, 6142–6154 (2001).
2. Breen, C. J., Raverdeau, M. & Voorheis, H. P. Development of a quantitative fluorescence-based ligand-binding assay. *Sci. Rep.* **6**, 1–9 (2016).
3. GraphPad. Fitting binding of fluorescent ligands. *KNOWLEDGEBASE - ARTICLE #1725* https://www.graphpad.com/support/faq/fitting-binding-of-fluorescent-ligands/ (2011).
4. Walsh, I., Seno, F., Tosatto, S. C. E. & Trovato, A. PASTA 2.0: An improved server for protein aggregation prediction. *Nucleic Acids Res.* **42**, 301–307 (2014).
5. Niu, M., Li, Y., Wang, C. & Han, K. RFAmyloid: A web server for predicting amyloid proteins. *Int. J. Mol. Sci.* **19**, (2018).